

Reaction–diffusion description of biological transport processes in general dimension

Cite as: J. Chem. Phys. **104**, 1918 (1996); <https://doi.org/10.1063/1.471810>

Submitted: 23 May 1995 . Accepted: 26 October 1995 . Published Online: 31 August 1998

W. Nadler, and D. L. Stein



View Online



Export Citation

ARTICLES YOU MAY BE INTERESTED IN

[Theory of reversible diffusion-influenced reactions](#)

The Journal of Chemical Physics **92**, 5270 (1990); <https://doi.org/10.1063/1.458533>

Lock-in Amplifiers

Find out more today



Zurich
Instruments

AIP
Publishing

Reaction–diffusion description of biological transport processes in general dimension

W. Nadler^{a)}

Institut für Theoretische Chemie, Universität Tübingen, Auf der Morgenstelle 8, D-72076 Tübingen, Germany

D. L. Stein^{b)}

Department of Physics, University of Arizona, Tucson, Arizona 85721

(Received 23 May 1995; accepted 26 October 1995)

We introduce a reaction–diffusion system capable of modeling ligand migration inside of proteins as well as conformational fluctuations of proteins, and present a detailed analytical and numerical analysis of this system in general dimension. The main observable, the probability of finding the system in the starting state, exhibits dimension-dependent as well as dimension-independent properties, allowing for sharp experimental tests of the effective dimension of the process in question. We discuss the application of this theory to ligand migration in myoglobin and to the description of gating fluctuations of ion channel proteins. © 1996 American Institute of Physics. [S0021-9606(96)50805-4]

I. INTRODUCTION

Several biological proteins have their active site not on their surface but, rather, buried deep inside the protein matrix. A central example are heme proteins where the ligand, a small gas molecule such as O₂ or CO, has to migrate through the protein matrix in order to reach its binding site. The motion of a ligand within a protein matrix is, therefore, a process of fundamental biological importance. Both the ligand binding and the ligand migration processes in myoglobin have been studied extensively,^{1–7} but a complete understanding of either is still lacking.

Early work¹ already made it clear that the problems involved were complicated, and that both ligand migration and binding kinetics are nontrivial. For example, both x-ray diffraction studies and molecular dynamics simulations⁸ revealed that ligand migration could not occur within a static protein in an “average” conformation—fluctuations are essential to open voids large enough through which the ligand can travel.³ Other complications include the ligand affecting the medium through which it travels, anisotropy and inhomogeneity of the protein matrix, and solvent interactions with the protein.

Because of the protein’s inhomogeneity, it is reasonable to suppose that voids occur only in preferred locations. Since the ligand cannot leave a site until a conformational fluctuation opens a nearby void, one could conclude that the internal ligand path is effectively one-dimensional. By one-dimensional, we mean that the ligand always retraces its previous path when it reverses its direction of motion. However, whether the actual ligand path in myoglobin is one- or higher-dimensional has not yet been resolved. On the other hand, the experimentally obtained time,¹ temperature,^{1,4} and pressure⁷ dependencies of ligand diffusion can be interpreted and understood correctly only with this information. It is also

necessary for a deeper insight into protein-internal fluctuations and their effects. Understanding the ligand migration process therefore requires, *as a prerequisite*, a determination of the dimensionality of the ligand path.

Experimental studies of this process have employed a variety of techniques. One of the oldest, and still most widely used, of these is the technique of flash photolysis.¹ Ligands bound to the heme site are separated by a pulse of laser light. The number $N(t)$ of unrecombined ligands at time $t > 0$ is then monitored. In some cases, rebinding occurs almost immediately. In others, the ligand wanders through the protein matrix for a while before recombining with the heme group. In the usual glycerol–water solvent, the latter process requires temperatures above roughly 170 K; below that, the solvent’s (and possibly the protein’s) glass transition freezes out the necessary conformational fluctuations. We note also that the ligand rebinding process per se appears to be coupled to protein relaxation processes.^{9,10}

When ligand migration does occur, it is typically seen to exhibit a $t^{-1/2}$ behavior for a range of temperature and time scales, before crossing over to an exponential at longer times.¹¹ Because the probability of return to the starting point in a $1d$ random walk falls off as $t^{-1/2}$, the observed behavior has been taken as an indication that ligand migration in myoglobin could be a one-dimensional diffusion process.¹²

In a previous paper,^{13,14} we showed that this conclusion is incorrect for a number of reasons. First of all, the behavior of the observable $N(t)$ is different from the probability of return to the origin; see also Sec. II of this paper. More importantly, however, modeling ligand migration through the protein matrix as diffusion in a d -dimensional shell and using boundary conditions appropriate for the actual biological situation, we find that the falloff for $N(t)$ is $t^{-1/2}$ during intermediate times *independent* of space dimension. We proposed a new, clear-cut experimental test, capable of distinguishing higher-dimensional from one-dimensional behavior—the presence (or absence) of a plateau region be-

^{a)}E-mail: walter.nadler@uni-tuebingen.de

^{b)}E-mail: dls@physics.arizona.edu

tween the algebraic decay regime and the exponential decay regime. This may already have been observed in the first extensive published study of the problem,¹ indicating that the diffusion path is actually three dimensional.

We have already indicated that—ultimately—the migration of a ligand inside the protein matrix has to be viewed as diffusion in a fluctuating environment. We note that work on this aspect of the problem has already begun with our study of diffusion on a fluctuating lattice.¹⁵ We show there (see also earlier work^{16–21}) that the effect of fluctuations is mainly to renormalize the effective diffusion coefficient, and we provide a simple renormalization group procedure for computing it in one dimension. Because the effective diffusion coefficient depends both on the average probability of a channel between neighboring sites being present, and on the correlation time of the opening and closing fluctuations of a channel, an understanding of this problem is essential for interpreting temperature and pressure dependencies of the diffusion process. It is not needed, however, for an understanding of the time dependence. Since we are concerned here only with the time-dependence of diffusion, this fact allows us to study the more standard diffusion problem below, and we will leave a study of temperature- and pressure-dependence to a future paper.

In this paper we continue and extend our theoretical study, providing new evidence for our conclusions and supplying details omitted in Ref. 13. The generic mathematical model we introduced there for the description of ligand migration processes—free diffusion in a d -dimensional shell with appropriate boundary conditions—will be analyzed in detail. It is surprising that the general behavior of such a relatively simple diffusion model has not, to our knowledge, been analyzed before, apart from some special cases.^{22–24}

The reaction–diffusion model we will discuss here is of a much more general character than the initial motivation, to describe ligand migration in proteins, suggests. It will be demonstrated that it can also be viewed as a simple generic microscopic model for the fluctuations of a protein between different macroscopic states. Therefore, we will consider it not only in one, two and three dimensions, necessary for investigating the path dimensionality in ligand migration. Rather, since the relevant state space of such complicated systems like biopolymers is expected to have a high dimensionality, we will try to explore the features of our model also in much higher dimensions. It will be seen that the features noticed in two and three dimensions will be much more pronounced in higher dimensions.

The plan of the paper is as follows:

In Sec. II we introduce the reaction–diffusion model¹³ which serves as a basis for studying the time-dependence of ligand diffusion in heme proteins.

In Sec. III we study the problem analytically. We solve it exactly for special boundary conditions in one and three dimensions and use Laplace transform methods to examine the eventual onset of dimension-dependent decay.

In Sec. IV we present detailed numerical studies, based on eigenfunction expansions, for general dimensions. We demonstrate the ubiquity of the $t^{-1/2}$ law for boundary con-

ditions corresponding to biological parameters, and find the appearance of the plateau region in dimensions greater than one. We complement these numerical studies with an analytical proof of the $t^{-1/2}$ decay in any dimension for appropriate boundary conditions. We also examine there the connection between our observed plateau and Polya's result of nonreturn to the origin for random walks in dimensions greater than two.²⁵

In Sec. V we present a generalized moment analysis^{26–28} which provides an alternative method for studying the plateau regime and the long-time aspects of decay. This analysis reinforces our earlier conclusions, and provides additional insights into the detailed behavior of the decay. It also supplies us with a simple means of determining under what conditions the onset of the plateau can occur.

In Sec. VI we will discuss in more detail the applicability of our model and our results to the description of general state space fluctuations of proteins. Of particular interest here are opening fluctuations of ion channel proteins. It will be seen that the principal observable in the ligand migration case is closely related to the closing time distributions of these proteins.

A discussion of our results, including their structural stability with respect to changes in boundary conditions and lack of isotropy, and our final conclusions will appear in Sec. VII.

II. THE MODEL

As indicated in the Introduction, we will describe the migration of a ligand through protein matter in globular proteins as a free diffusion process in a d -dimensional shell. In doing so, the protein matrix is assumed implicitly to be homogeneous and isotropic. Although this simplifying assumption might seem at first to be wholly inappropriate for proteins, many general conclusions that can be drawn from our results are completely unaffected by it; see the final discussion in Sec. VII.

The physical situation of an active site inside a globular protein is sketched in Fig. 1. Assuming spherical symmetry for the protein, the active site, and its location inside the protein, we can disregard any angular degrees of freedom. The diffusion equation for the radial probability distribution $p(r, t)$ of the ligand is then

$$\frac{\partial}{\partial t} p(r, t) = D \left[\frac{\partial^2}{\partial r^2} + \frac{d-1}{r} \frac{\partial}{\partial r} \right] p(r, t). \quad (2.1)$$

Since the motion of a ligand through the dense protein matrix has to be facilitated by protein internal fluctuations, the motion of the ligand is actually coupled to the opening and closing of local channels and/or the creation of local free volumes. As discussed in the Introduction, such processes result mainly in a renormalization of the effective diffusion coefficient D .¹⁵ Therefore, the diffusion coefficient D in Eq. (2.1) has to be considered to be renormalized with respect to these local channel/free volume fluctuations within the protein matrix. The value of D will depend on the interplay between the time scale of measurement and the rate of physi-

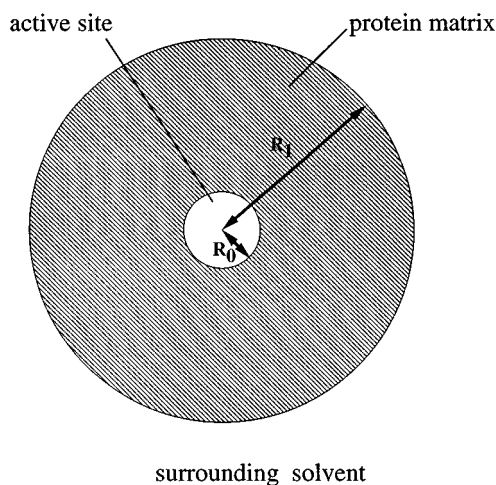


FIG. 1. Sketch of the ligand migration problem.

cally relevant fluctuations, and, therefore, on temperature, pressure, and other environmental parameters experienced by the protein.

One boundary condition for Eq. (2.1) arises from the ligand binding process which takes place at the active site within the protein. Ligands are assumed to be absorbed with a specified rate γ upon arrival at the site, i.e.,

$$\frac{d}{dt} N(t) = -\gamma p(R_0, t), \quad (2.2)$$

where R_0 is the size of the active site, which, in the case of myoglobin, is of the order of the size of the heme cavity, i.e., several Å. In Eq. (2.2), $N(t)$ is the number of ligands still in the protein matrix,

$$N(t) = \int_{R_0}^{R_1} dr r^{d-1} p(r, t), \quad (2.3)$$

and this is also the main observable that is monitored experimentally when investigating the rebinding process. Using the radial probability current,

$$j(r, t) = -D \frac{\partial}{\partial r} p(r, t), \quad (2.4)$$

the absorption Eq. (2.2) follows from the reactive boundary condition

$$j(R_0, t) = -\gamma p(R_0, t), \quad (2.5)$$

for Eq. (2.1).

The reactive boundary condition (2.5) can be extended readily to more general situations, including nonexponential rebinding arising from (i) proteins frozen into conformational substates, giving rise to a distribution $g(\gamma)$ of rate coefficients γ , or (ii) the rebinding process being dynamically coupled to other degrees of freedom, giving rise to a fluctuating rate coefficient $\gamma(t)$. These complications, however, are unlikely to play a significant role at temperatures and time scales in which diffusion of the ligand through the protein

matrix makes an important contribution to the observed rebinding curve, and, therefore, we confine our attention to Eq. (2.5).

The outer boundary connects the protein matrix with the surrounding solvent. In this contribution we will be concerned mainly with two different physical situations; (i) the low temperature regime where the solvent is frozen, i.e., no ligand can escape into the solvent, and (ii) the concentration of ligands in the protein is kept constant, namely one per protein, so that no net flux across the protein-solvent interface arises. Both situations are often realized experimentally, and both are of great interest.¹ Conveniently, both situations give rise to the same mathematical description—a zero flux or reflective boundary condition at some radius R_1 , which corresponds to the outer radius of the protein,

$$j(R_1, t) = 0. \quad (2.6a)$$

In the most general experimental situation, however, a time-varying nonzero flux of ligands across the protein-solvent interface could be possible. Depending on the actual situation, the exchange of ligands between the protein and the solvent could be described by a variety of equations. For example, a reactive condition like Eq. (2.5) on the outer boundary would describe an effective leakage of ligands into the solvent with some rate, which is possible, e.g., when the ligand concentration in the solvent is kept practically at zero. The mathematics of a model with a reactive outer boundary condition is only slightly different from what we consider here, albeit much more tedious. We will show that the general conclusions drawn from our results are largely insensitive to the form of the outer boundary condition by considering also two special cases, namely a reactive boundary with the *same* reaction coefficient as in Eq. (2.5),

$$j(R_1, t) = \gamma p(R_1, t), \quad (2.6b)$$

—note the sign change with respect to Eq. (2.5) due the different directions of the outflux at the inner and outer boundary—and a fully absorptive boundary,

$$p(R_1, t) = 0. \quad (2.6c)$$

In this way we will be able to see the full spectrum of possible dynamical behavior resulting from different boundary conditions, without introducing any additional parameters. Equation (2.6b) is—together with Eq. (2.6a)—of particular importance for the interpretation of the model in terms of state space fluctuations of proteins; see Sec. VI below, while Eq. (2.6c) corresponds to a complete loss of the ligand into the medium upon reaching the protein-solvent interface.

Finally, we use the initial condition

$$p(r, 0) = \delta(r - R_0) / r^{d-1}, \quad (2.7)$$

which facilitates direct comparison of our model with flash photolysis experiments. The ligand enters the diffusion volume at R_0 , i.e., at the inner shell, where it can either rebind immediately with rate γ to the active site, or diffuse into the protein matrix and be rebound later.

We can eliminate the dimensional constants D and γ immediately by rescaling our space and time variables with

the reactive time- and length scales $\tau_r = D/\gamma^2$ and $l_r = D/\gamma$. The new dimensionless variables are then gotten from the transformation $t \rightarrow t/\tau_r$ and $r \rightarrow r/l_r$. These dimensionless variables will be used in the remainder of this paper. Our rescaled diffusion equation is then

$$\frac{\partial}{\partial t} p(r,t) = \left[\frac{\partial^2}{\partial r^2} + \frac{d-1}{r} \frac{\partial}{\partial r} \right] p(r,t), \quad (2.8)$$

with the inner boundary condition

$$\left. \frac{\partial}{\partial r} p(r,t) \right|_{r=R_0} = p(R_0,t), \quad (2.9)$$

and with the respective outer boundary conditions

$$\left. \frac{\partial}{\partial r} p(r,t) \right|_{r=R_1} = 0, \quad (2.10a)$$

$$\left. \frac{\partial}{\partial r} p(r,t) \right|_{r=R_1} = p(R_1,t), \quad (2.10b)$$

$$p(R_1,t) = 0. \quad (2.10c)$$

The initial condition, Eq. (2.7), remains unchanged.

The rescaling leaves us with three dimensionless parameters for our model; the space dimension d , and the—now dimensionless—inner and outer shell radii, R_0 and R_1 . Note that all explicit dependencies on the diffusion and the reaction coefficient have dropped out of the system (2.7)–(2.10). As already noted in the Introduction and to be discussed more thoroughly below in Sec. VI, the model defined by Eqs. (2.7)–(2.10) can be viewed equally well as describing the internal fluctuations of a system with a d -dimensional state space, with d possibly large. We will therefore analyze the behavior of this model for general d .

III. EXACT RESULTS

In the following three subsections we will consider general isotropic diffusion with an inner reactive boundary only, i.e., we will consider the limit $R_1 \rightarrow \infty$. By studying the problem first analytically in the absence of an outer boundary and then, in Sec. IV, numerically with this boundary, we will be able to clarify the behavior induced by its presence.

We will demonstrate how in this limit the problem can be solved exactly in one and in three dimensions using Green's function techniques and the method of images. Although these results can be found—in principle—in the literature,^{29,30,31} we find it pedagogically helpful to rederive them here with our particular problem in mind. For general dimensions exact results can be obtained for the Laplace transforms of the observable $N(t)$. These results allow a systematic study of the long time behavior. Although analytical back transformation is not possible in general, it is possible in one and three dimensions and provides a complementary method for deriving the results obtained by the direct method.

A. Exact solution in one dimension

After the limit $R_1 \rightarrow \infty$ has been performed, the actual value of the inner boundary, R_0 , is not relevant anymore in one dimension, and we will set it to zero, for simplicity. Also, in order to distinguish this simplified one-dimensional from the higher-dimensional treatment, we will replace r by x here.

We can simplify the problem defined by Eqs. (2.8) and (2.9) further by introducing the auxiliary function

$$g(x,t) = p(x,t) - \frac{\partial}{\partial x} p(x,t). \quad (3.1)$$

It obeys the one-dimensional diffusion equation

$$\frac{\partial}{\partial t} g(x,t) = \frac{\partial^2}{\partial x^2} g(x,t) \quad (3.2)$$

along with the boundary condition

$$g(0,t) = 0. \quad (3.3)$$

In other words, g behaves like a probability density with an absorber at the origin. From the auxiliary function g the original distribution p can be reconstructed via

$$p(x,t) = e^x \int_x^\infty dx' e^{-x'} g(x',t), \quad (3.4)$$

which is the solution to Eq. (3.1), using the property that p vanishes at infinity. g itself will be determined from Eqs. (3.2) and (3.3) using Green's functions and the method of images.

Consider first a particle whose probability density $G(x,t)$ obeys just Eq. (3.2), i.e., diffusion on the infinite line, with the initial condition that at time zero the particle is found at some position x_0 , i.e., $G(x,0;x_0) = \delta(x-x_0)$. The probability density is then easily seen to be

$$G(x,t;x_0) = \frac{1}{\sqrt{4\pi t}} e^{-(x-x_0)^2/4t}, \quad (3.5)$$

which is simply the Green's function of Eq. (3.2).

Consider now a particle whose probability density $F(x,t)$ obeys Eqs. (3.2) and (3.3) with the initial condition that at time zero the particle is found at some *positive* position x_0 . That is, we are interested in diffusion on the positive half-infinite line with an absorptive boundary condition at the origin. The Green's function $G(x,t;x_0)$ would solve for the initial condition and the diffusion equation, but not for the boundary condition, Eq. (3.3). In the method of images, copies of the Green's function $G(x,t;x'_0)$ with starting points x'_0 *outside* of the domain of interest, which is here $(0,\infty)$, are added with appropriate weights so that the boundary condition can be satisfied. Choosing the starting points outside of the domain of interest guarantees that the added functions do not interfere with the initial condition. In our case, it is easily seen that choosing $x'_0 = -x_0$ and a relative weight of -1 for a single additional Green's function solves the problem. The resulting probability density has, therefore, the form

$$F(x,t;x_0) = G(x,t;x_0) - G(x,t;-x_0) \\ = \frac{1}{\sqrt{4\pi t}} [e^{-(x-x_0)^2/4t} - e^{-(x+x_0)^2/4t}]. \quad (3.6)$$

Moreover, F is the Green's function of Eq. (3.2) with boundary condition (3.3).

For the initial condition of the original probability density p we choose now the general form $p(x,0) = \delta(x-x_0)$, with x_0 again on the positive axis. Then the initial condition for the auxiliary function g is given by

$$g(x,0) = \delta(x-x_0) - \frac{\partial}{\partial x} \delta(x-x_0). \quad (3.7)$$

Now we can employ the well-known technique for computing the general solution from the Green's function, in this case F , and the particular initial condition,

$$g(x,t) = \int_0^\infty dx_0 F(x,t;x_0) g(x_0,0), \quad (3.8)$$

where the integral has to be evaluated with g interpreted as a generalized function.³² The full solution for g is then given by

$$g(x,t) = \int_0^\infty dx_0 \delta(x-x_0) \left(1 + \frac{\partial}{\partial x_0} \right) F(x,t;x_0) \\ = \frac{1}{\sqrt{4\pi t}} [e^{-(x-x_0)^2/4t} - e^{-(x+x_0)^2/4t}] + \left\{ \frac{1}{\sqrt{\pi t}} [(x \right. \\ \left. - x_0) \right. \\ \left. \times e^{-(x-x_0)^2/4t} + (x+x_0)e^{-(x+x_0)^2/4t}] \right\}. \quad (3.9)$$

The original distribution p is obtained by evaluating Eq. (3.4). After some algebra the answer can be simplified to

$$p(x,t;x_0) = \frac{1}{\sqrt{4\pi t}} [e^{-(x-x_0)^2/4t} + e^{-(x+x_0)^2/4t}] \\ - e^{x+x_0+t} \operatorname{erfc} \left[\frac{x+x_0+2t}{\sqrt{4t}} \right], \quad (3.10)$$

where erfc is the complementary error function.³³

Finally, setting the starting point to zero, i.e., $x_0=0$, brings us back to our model description of ligand migration. The unreacted fraction of ligands is then obtained from the integration in Eq. (2.3) to

$$N_{1d}(t) = e^t \operatorname{erfc}(\sqrt{t}). \quad (3.11)$$

Using the behavior of erfc for large values of the argument,³³ it is easy to show that $N_{1d}(t)$ exhibits an asymptotic algebraic $t^{-1/2}$ decay after an initial transient of order $t \approx 1$,

$$\lim_{t \rightarrow \infty} N_{1d}(t) \rightarrow \sqrt{\frac{1}{\pi t}} + O(t^{-3/2}). \quad (3.12)$$

B. Exact solution in three dimensions

Again we introduce the auxiliary function g , defined in Eq. (3.1), which, this time, has to obey the three-dimensional radial diffusion equation

$$\frac{\partial}{\partial t} g(r,t) = \frac{\partial^2}{\partial r^2} g(r,t) + \frac{2}{r} \frac{\partial}{\partial r} g(r,t), \quad (3.13)$$

together with the boundary condition

$$g(R_0,t) = 0. \quad (3.14)$$

Also, for the initial condition of the original distribution we choose $p(r,0) = \delta(r-r_0)/r^2$, with $r_0 \leq R_0$. Then the initial condition for g has the form

$$g(r,0) = \delta(r-r_0)/r^2 - \frac{\partial}{\partial r} \delta(r-r_0)/r^2. \quad (3.15)$$

The original distribution p can—again—be reconstructed from g using Eq. (3.4).

We will use the Green's function technique for the final determination of g again. However, the derivation of a Green's function for Eqs. (3.13) and (3.14) is somewhat more complicated than it was in the one-dimensional case. Nevertheless, we will be able to utilize some of the results from the previous section.

Consider now a particle whose probability distribution $H(r,t)$ obeys Eqs. (3.13) and (3.14) and starts at a radius $r_0 > R_0$, i.e., it performs a free diffusion in the infinite shell with inner radius R_0 . First we introduce a new function $h(r,t)$ by the relation $H(r,t) = h(r,t)/r$. Then $h(r,t)$ satisfies

$$\frac{\partial}{\partial t} h(r,t) = \frac{\partial^2}{\partial r^2} h(r,t) \quad (3.16)$$

which is the simple one-dimensional diffusion equation. This immediately implies that one solution to Eq. (3.13) is proportional to $G(r,t;r')/r$ for some fixed r' , with G being the one-dimensional Green's function. However, this cannot by itself be the solution for a freely diffusing particle; it is easily seen that the integrated probability density diverges as $t \rightarrow \infty$. The presence of an absorbing boundary Eq. (3.14) is helpful here and allows us to use the method of images again. Adding two one-dimensional Green's functions $G(r,t;r')$, one centered at $r' = r_0$ with weight $+1$ and one centered at $r' = -(r_0 - 2R_0)$ with weight -1 satisfies the boundary condition (3.14) and the initial condition in the domain (R_0, ∞) . The final form of the three-dimensional radial Green's function H is then

$$H(r,t;r_0) = \frac{1}{rR_0} \{G(r,t;r_0) - G[r,t;-(r_0-2R_0)]\}, \quad (3.17)$$

and it turns out that satisfying the boundary condition solves the divergence problem; the divergent parts cancel and the integrated probability density of this function is bounded from above by unity.

Let us pause here for a moment and investigate some properties of the diffusion process described by the Green's

function H . The fraction of particles remaining at time t in the shell $r > R_0$ is given after spatial integration by

$$N_H(t) = 1 - \frac{R_0}{r_0} \operatorname{erfc}\left(\frac{r_0 - R_0}{\sqrt{4t}}\right). \quad (3.18)$$

Asymptotically for long times this becomes

$$\lim_{t \rightarrow \infty} N_H(t) \rightarrow \frac{r_0 - R_0}{r_0} \left[1 + \frac{R_0}{\sqrt{\pi t}} + O(t^{-3/2}) \right]. \quad (3.19)$$

We again obtain the $t^{-1/2}$ decay at long times—in fact, it takes over rather quickly, after an initial transient. A new feature has appeared, however. In one dimension we saw that the decay continues indefinitely, tending toward zero (all particles absorbed) at long times. In three dimensions, however, even with a fully absorptive boundary condition at R_0 , the decay tends towards a nonzero constant; only a fraction of the particles is absorbed, no matter how long the diffusion process continues. This is a manifestation of the famous Polya theorem,²⁵ which states that for symmetric random walks on discrete lattices in one and two dimensions, the diffusing particle will return infinitely often to the origin. In three and higher dimensions, however, the probability that the particle will return to its starting point is strictly less than one—on a three-dimensional cubic lattice, this probability is approximately 0.35. Roughly speaking, in these higher dimensions the space in which the particle wanders is large enough so that there is a nonzero chance that the particle can get “lost.”

For continuous-time and -space random walks, as discussed here, the theorem can be modified to a statement of whether the particle returns to an arbitrarily small neighborhood of its starting point. Our calculation shows that, in the problem discussed above, the probability of the particle hitting the absorbing sphere is R_0/r_0 . Note that for $r_0 = R_0$, i.e., the particle starts on the absorbing sphere itself, $N(t)$ is zero for all time; for $R = 0$, $N(t) = 1$ for all time. The latter simply follows from the fact that, although in a continuous-space random walk there is a nonzero probability for the particle to come arbitrarily close to the origin, there is zero probability of it actually hitting any prespecified point.

We will see in later sections that the Polya theorem will play an important role in understanding the dimension-dependent behavior of ligand diffusion.

The auxiliary function g is, finally, obtained using the Green's function H and the initial condition, Eq. (3.15). Note that in three dimensions the corresponding equation differs somewhat from Eq. (3.8), due to the existence of the three-dimensional volume element r_0^2 ,

$$g(r, t) = \int_{R_0}^{\infty} dr_0 r_0^2 H(r, t; r_0) g(r_0, 0). \quad (3.20)$$

We skip now the tedious algebra involved in evaluating this relation, reconstructing the original distribution p via Eq. (3.4), going to the limit $r_0 \rightarrow R_0$ to obtain our ligand migra-

tion model and evaluating the fraction of unreacted ligands, since nothing is involved that is conceptually new. The final result is

$$N_{3d}(t) = 1 - \frac{R_0}{R_0 + 1} \left\{ 1 - \exp\left[\left(\frac{R_0 + 1}{R_0}\right)^2 t\right] \operatorname{erfc}\left(\frac{R_0 + 1}{R_0} \sqrt{t}\right) \right\}, \quad (3.21)$$

with the asymptotic long-time behavior

$$\lim_{t \rightarrow \infty} N_{3d}(t) \rightarrow 1 - \frac{R_0}{R_0 + 1} \left[1 - \frac{R_0}{R_0 + 1} \frac{1}{\sqrt{\pi t}} + O(t^{-3/2}) \right]. \quad (3.22)$$

Again, we recognize the Polya behavior, $N_{3d}(\infty) = 1/(R_0 + 1)$, this time for a reactive inner shell, not a fully absorptive one as in Eq. (3.19). For large inner shells, i.e., R_0 large on the diffusive length scale l_r , the escape probability vanishes as $N_{3d}(\infty) \propto 1/R_0$, while for small R_0 the escape probability goes to unity.

C. Laplace transform results

In general dimensions it is not possible to get exact solutions to the problem of isotropic diffusion with an inner reactive boundary. Analytical progress in studying the general problem can be made, however, by using Laplace transform techniques. In this section we use the methods introduced by Tachiya²² and Sano and Tachiya.³⁴

We again consider a particle isotropically diffusing in d dimensions and confined to the domain $R_0 \leq r < \infty$. Its radial probability density $p(r, t)$ satisfies (we use dimensionless time and space variables as described in the previous section)

$$\frac{\partial}{\partial t} p(r, t) = \nabla^2 p(r, t), \quad (3.23a)$$

where $\nabla^2 = (\partial^2/\partial r^2) + [(d-1)/r](\partial/\partial r)$. The inner reactive boundary is described by the condition

$$\frac{\partial}{\partial r} p(r, t) \Big|_{r=R_0} = p(R_0, t) \quad (3.23b)$$

and we assume that the particle starts at some radial position $r_0 > R_0$,

$$p(r, 0) = \delta(r - r_0)/r_0^{d-1}. \quad (3.23c)$$

Define the Laplace transform $\tilde{p}(r, s)$ with respect to time in the usual way,

$$\tilde{p}(r, s) = \int_0^{\infty} dt e^{-st} p(r, t). \quad (3.24)$$

The diffusion Eq. (3.23a) then becomes

$$\nabla^2 \tilde{p} - s \tilde{p} = -\delta(r - r_0)/r_0^{d-1}. \quad (3.25)$$

Sano and Tachiya³⁴ make the following useful observation: Eq. (3.25) is a Green's function equation, and its reciprocity property can be utilized to arrive at the adjoint equation of (3.25),

$$\nabla_{r_0}^2 \tilde{p}(r, s; r_0) - s\tilde{p}(r, s; r_0) = -\delta(r - r_0)/r_0^{d-1}, \quad (3.26)$$

where $\nabla_{r_0}^2$ is the Laplacian operating on the variable r_0 , and the dependence of \tilde{p} on r_0 is now explicitly noted. Now define

$$N(r_0, t) = \int_{R_0}^{\infty} dr r^{d-1} p(r, t; r_0). \quad (3.27)$$

Integrating Eq. (3.26) over $\int_{R_0}^{\infty} dr r^{d-1}$, we get

$$\nabla_{r_0}^2 \tilde{N}(r_0, s) - s\tilde{N}(r_0, s) = -1. \quad (3.28)$$

It is also easy to show that Eq. (3.23b) becomes

$$\left. \frac{\partial}{\partial r_0} \tilde{N}(r_0, s) \right|_{r_0=R_0} = \tilde{N}(R_0, s) \quad (3.29)$$

and that

$$\lim_{r_0 \rightarrow \infty} \tilde{N}(r_0, s) = 1/s. \quad (3.30)$$

We can simplify slightly by writing $\tilde{N}(r_0, s) = r_0^{1-d/2} \psi(r_0, s)$ and plugging into Eq. (3.28). The resulting homogeneous equation for $\psi(r_0, s)$ has as its solutions the modified Bessel functions³³ $I_{\pm(1-d/2)}(\sqrt{s}r_0)$ and $K_{d/2-1}(\sqrt{s}r_0)$. Any two of these form a linearly independent pair; relations among the three are given in Abramowitz and Stegun.³³ (They are slightly different if the functions are of integer order or of half-integer order.) However, $I_{\pm\nu}(z)$ diverges as $z \rightarrow \infty$ regardless of whether ν is an integer or half-integer, and $K_{\nu}(z) \rightarrow 0$ as $z \rightarrow \infty$. Our solution to Eqs. (3.28) and (3.29) is then

$$\tilde{N}(r_0, s) = C r_0^{1-d/2} K_{d/2-1}(\sqrt{s}r_0) + 1/s, \quad (3.31)$$

where C is a constant to be determined. This is easily done by using the boundary condition (3.29), so the full (exact) solution to Eqs. (3.28)–(3.30) is

$$\begin{aligned} \tilde{N}(r_0, s) = & \frac{1}{s} \left\{ 1 - \left(\frac{r_0}{R_0} \right)^{1-d/2} \right. \\ & \times \left[\frac{1}{1 + \sqrt{s} \frac{K_{d/2}(\sqrt{s}R_0)}{K_{d/2-1}(\sqrt{s}R_0)}} \right] \frac{K_{d/2-1}(\sqrt{s}r_0)}{K_{d/2-1}(\sqrt{s}R_0)} \left. \right\}. \end{aligned} \quad (3.32)$$

For $d=1, 2$, and 3 , this agrees exactly with the results of Sano and Tachiya (Table I).³⁴

We are most interested in the case where $r_0=R$; this simplifies Eq. (3.32) considerably to

$$\tilde{N}(R, s) = \frac{1}{s} \left\{ 1 - \frac{1}{1 + \sqrt{s} \frac{K_{d/2}(\sqrt{s}R_0)}{K_{d/2-1}(\sqrt{s}R_0)}} \right\}. \quad (3.33)$$

By using the fact that the limit $t \rightarrow \infty$ corresponds to $s \rightarrow 0$ for the Laplace transform, we can use these equations to analyze

the long-time limit and illustrate how the Polya theorem works in this model. For $\nu > 0$, and in the limit $z \rightarrow 0$, $K_{\nu}(z) \sim \frac{1}{2}\Gamma(\nu)(\frac{1}{2}z)^{-\nu}$ [note that $K_{\nu}(z) = K_{-\nu}(z)$].³³ Then in one dimension, the right-hand side of Eq. (3.33) tends to $1/\sqrt{s}$ in the limit $s \rightarrow 0$, which corresponds to a long-time decay $N(t) \sim t^{-1/2}$.

Two dimensions is a special case; here we need the limiting form $K_0(z) \sim -\log z$ for small z . Using this in Eq. (3.33) yields $\tilde{N}(R_0, s) \rightarrow (-1/s \log s)$ as $s \rightarrow 0$; the decay is marginal. For long times, $N(t)$ decays as $1/\log t$.

In three and higher dimensions Polya's theorem ensures that \tilde{N} will grow as $1/s$ as $s \rightarrow 0$; that is, $N(t)$ tends towards a constant as $t \rightarrow \infty$. We find that as $s \rightarrow 0$, $\tilde{N}(R, s) \rightarrow (1/s)(d-2/d-2+R_0)$, so that as $t \rightarrow \infty$,

$$N(R_0, t) \rightarrow \frac{d-2}{R_0+d-2}, \quad d \geq 3. \quad (3.34)$$

We can find the inverse transform of Eq. (3.32) and solve exactly for the general case ($r_0 \geq R$) in one and three dimensions. In one dimension we find

$$\begin{aligned} N_{1d}(r_0, t) = & 1 - \left[\operatorname{erfc} \left(\frac{r_0 - R_0}{2\sqrt{t}} \right) - e^{(r_0 - R_0)} e^{-t} \right. \\ & \left. \times \operatorname{erfc} \left(\sqrt{t} + \frac{r_0 - R_0}{2\sqrt{t}} \right) \right]. \end{aligned} \quad (3.35)$$

When $r_0=R_0$ this reduces to Eq. (3.11).

In three dimensions

$$\begin{aligned} N_{3d}(r_0, t) = & 1 - \frac{R_0}{r_0} \frac{1}{1 + \frac{1}{R_0}} \left\{ \operatorname{erfc} \left(\frac{r_0 - R_0}{2\sqrt{t}} \right) \right. \\ & \left. - e^{(1+1/R_0)(r_0 - R_0)} e^{(1+1/R_0)^2 t} \right. \\ & \left. \times \operatorname{erfc} \left[\left(1 + \frac{1}{R_0} \right) \sqrt{t} + \frac{r_0 - R_0}{2\sqrt{t}} \right] \right\}. \end{aligned} \quad (3.36)$$

As $t \rightarrow \infty$, this becomes

$$N_{3d}(r_0, t) = 1 - \frac{R_0}{r_0} \frac{1}{1 + \frac{1}{R_0}} \left[1 - \frac{1}{\sqrt{\pi}} \frac{e^{(1+1/R_0)(r_0 - R_0)}}{1 + \frac{1}{R_0}} t^{-1/2} \right] \quad (3.37)$$

so the Polya limit is $N(r_0, \infty) = 1 - (R_0/r_0)[1/1 + (1/R_0)]$. For $r_0=R_0$ we recover Eq. (3.22).

An important consequence of Eq. (3.32) is that the decay of $N(r_0, t)$ leading to the Polya regime will be dimension-dependent in general. By keeping higher-order terms in the small- s expansion of the modified Bessel functions, Eq. (3.32) can be used to study this behavior in detail. This can get rather messy, however, so we report on only one important aspect of the general dynamics. For $r_0 \gg R_0$, $N(r_0, t)$ remains close to one until about the time it takes for the

particle to diffuse to the reactive boundary, which is of order $(r_0 - R_0)^2$. Long after that time, the fraction of particles remaining decays as $t^{-(d-2)/2}$ (for $d \geq 3$) towards the Polya limit.

The decay behavior is very different for $r_0 \approx R_0$, however. There the decay sets in quickly, of course, and after an initial transient decays as $t^{-1/2}$. This is because the geometry looks quasi-one-dimensional for the particle close to the reactive boundary. While there may be some dimension-dependent behavior near the onset of the Polya regime, this in general will not be noticeable for r_0 close to or equal to R_0 —the Polya regime sets in before the dimension-dependent regime becomes appreciable. In these cases, the behavior looks remarkably dimension-independent; aside from the initial transient, one sees a $t^{-1/2}$ decay towards a nonzero constant. Because measurements of ligand diffusion correspond to the initial condition $r_0 = R_0$, this has important consequences for measurements of ligand recombination, as discussed in Ref. 13. This point will be dealt with further in Secs. IV and V.

IV. NUMERICAL TREATMENT AND RESULTS

We will present in the following a detailed numerical treatment of the problem defined by Eqs. (2.7)–(2.10). First, we will describe the numerical procedure involved, and discuss its effective implementation. In Sec. IV B we will present extensive numerical results that show the existence of an intermediate algebraic decay of $N(t)$, with $t^{-1/2}$, together with the existence of a plateau-regime in $d > 1$. In Sec. IV C, we will present a mathematical argument for the existence of the algebraic regime, and, finally, in Sec. IV A we will analyze the relationship between the plateau regime and the properties of the lowest eigenvalues.

A. Numerical solution

Equation (2.8) with initial condition (2.7) can be solved via a spectral expansion

$$p(r, t) = \sum_n \exp(-k_n^2 t) \psi_n(r) \psi_n(R_0), \quad (4.1)$$

where the $\psi_n(r)$ are the eigenfunctions of the right-hand side differential operator in Eq. (2.8), with eigenvalues $-k_n^2$. Using standard Sturm–Liouville theory³⁵ it can be shown that these eigenfunctions obey the orthogonality relation

$$\int_{R_0}^{R_1} dr r^{d-1} \psi_n(r) \psi_m(r) = \delta_{n,m} N^2, \quad (4.2)$$

with N being a normalization constant. For general d the eigenfunctions can be expressed in terms of Bessel functions,

$$\psi_n(r) = r^{1-d/2} [a_n J_{1-d/2}(k_n r) + b_n Y_{1-d/2}(k_n r)], \quad (4.3)$$

where J and Y are the (linearly independent) Bessel functions of the first and second kind, respectively.³³ In odd dimensions, i.e., for half-integer indices, these Bessel functions are related to their spherical counterparts, and can be repre-

sented using polynomials in $1/r$ and trigonometric functions. In one dimension they are simply given by the sine and cosine functions.

The eigenvalues k_n , together with the amplitudes a_n and b_n , can now be determined from the boundary conditions (2.9) and (2.10). In order to apply these boundary conditions, we use the standard formula³⁶

$$\frac{d}{dy} [y^\nu Z_\nu(y)] = y^\nu Z_{\nu-1}(y), \quad (4.4)$$

where Z represents either Bessel function J or Y .³³ Then the inner reactive boundary condition Eq. (2.9) becomes

$$\begin{aligned} k_n [a_n J_{-d/2}(k_n R_0) + b_n Y_{-d/2}(k_n R_0)] \\ = a_n J_{1-d/2}(k_n R_0) + b_n Y_{1-d/2}(k_n R_0). \end{aligned} \quad (4.5)$$

Similarly, the outer reflecting boundary condition, Eq. (2.10a), becomes

$$a_n J_{-d/2}(k_n R_1) + b_n Y_{-d/2}(k_n R_1) = 0. \quad (4.6)$$

It is useful at this stage to transform to new parameters, the width of the shell

$$\Delta R = R_1 - R_0, \quad (4.7a)$$

and the ratio of this shell width to the inner radius

$$X = \frac{\Delta R}{R_0}, \quad (4.7b)$$

and to introduce the scaled eigenvalue

$$K_n = k_n \Delta R. \quad (4.8)$$

Eliminating the amplitudes a_n and b_n using the two Eqs. (4.5) and (4.6), and employing the parameters introduced above, we derive the eigenvalue equation for K_n in arbitrary dimension,

$$\begin{aligned} 0 = & J_{1-d/2} \left(K_n \frac{1}{X} \right) Y_{-d/2} \left[K_n \frac{X}{(1+X)} \right] \\ & - J_{-d/2} \left[K_n \frac{X}{(1+X)} \right] Y_{1-d/2} \left(K_n \frac{1}{X} \right) \\ & - \frac{K_n}{\Delta R} \left\{ J_{-d/2} \left(K_n \frac{1}{X} \right) Y_{-d/2} \left[K_n \frac{X}{(1+X)} \right] \right. \\ & \left. - J_{-d/2} \left[K_n \frac{X}{(1+X)} \right] Y_{-d/2} \left(K_n \frac{1}{X} \right) \right\}. \end{aligned} \quad (4.9)$$

In one dimension, for example, this equation simplifies to

$$\cos(K_n) - \frac{K_n}{\Delta R} \sin(K_n) = 0. \quad (4.10)$$

The motivation for the parameter transformation (4.7)–(4.8) is easily seen now. In one dimension the eigenvalue equation assumes a very simple form. Furthermore, we will be concerned below very often with the regime of large ΔR . In this regime, the low-lying eigenvalues, i.e., $K_n \ll \Delta R$, which determine the long-time behavior, can be determined with sufficient accuracy by neglecting the second term in the

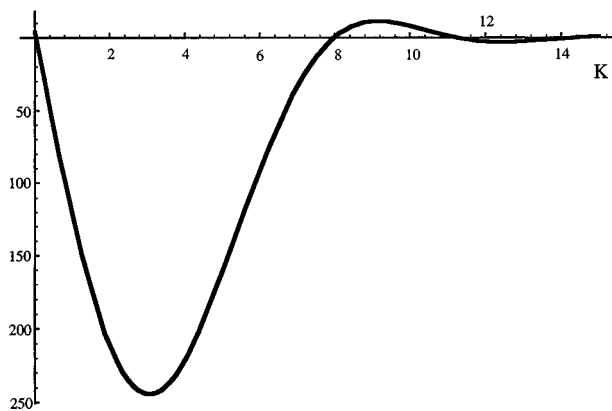


FIG. 2. Function defined by the left-hand side of Eq. (4.9) for $d=10$, $\Delta R=10^3$, and $X=10$; the zeros of this function are the eigenvalues k_n entering the eigenfunction expansion (4.1).

equations. On the other hand, the eigenvalues that determine the short-time behavior, i.e., $K_n \gg \Delta R$, can be obtained by neglecting the first term in the inverse equations, i.e.,

$$0 = \frac{\Delta R}{K_n} \left\{ J_{1-d/2} \left(K_n \frac{1}{X} \right) Y_{-d/2} \left[K_n \frac{X}{(1+X)} \right] - J_{-d/2} \left[K_n \frac{X}{(1+X)} \right] Y_{1-d/2} \left(K_n \frac{1}{X} \right) \right\} - \left\{ J_{-d/2} \left(K_n \frac{1}{X} \right) Y_{-d/2} \left[K_n \frac{X}{(1+X)} \right] - J_{-d/2} \left[K_n \frac{X}{(1+X)} \right] Y_{-d/2} \left(K_n \frac{1}{X} \right) \right\} \quad (4.9')$$

and

$$\frac{\Delta R}{K_n} \cos(K_n) - \sin(K_n) = 0. \quad (4.10')$$

In both limits, $K_n \gg \Delta R$ and $K_n \ll \Delta R$, the eigenvalue equations for the K_n become independent of ΔR , and consequently, this holds also for the corresponding K_n . This property gives us already some insight into the scaling behavior of the time constants $1/k_n^2$; see Eq. (4.1). For large values of ΔR those time constants will scale with ΔR^2 , which is particularly important for the longest time scales.

The zeros of the left-hand side function in Eq. (4.9) are the eigenvalues of the spectral expansion. Figure 2 shows the typical behavior of that function which exhibits the qualitative characteristics known from Bessel functions. There is the practical problem of finding these zeros in an effective way. For the case of the lowest eigenvalue one can utilize the results of the generalized moment treatment of Sec. V below, namely that the inverse of the time constant τ_l , which is given in analytical form, provides an exact upper limit for the lowest eigenvalue k_1^2 . This upper limit can be used in any numerical scheme³⁷ as the interval $(0, \sqrt{1/\tau_l}]$ in which to perform the numerical search for that eigenvalue.

For the higher-lying eigenvalues there arises the problem of specifying intervals in which to look for the eigenvalues, without overlooking one. This is particularly a major problem for the determination of the second eigenvalue, K_2 . As can be seen already in Fig. 2, and will be discussed in more detail below in Sec. IV D, there emerges a considerable gap which increases with dimension.

For still higher eigenvalues, however, one can use the following arguments. Let us consider the regime $K_n \gg \max[X, (1+X/X)]$. Using the properties of Bessel functions for large values of the argument,³⁶

$$J_{\pm \nu}(z) = \sqrt{\frac{2}{\pi z}} \cos\left(z \mp \frac{\pi}{2} \nu - \frac{\pi}{4}\right) + O(1/z), \quad (4.11a)$$

and

$$Y_{\pm \nu}(z) = \sqrt{\frac{2}{\pi z}} \sin\left(z \mp \frac{\pi}{2} \nu - \frac{\pi}{4}\right) + O(1/z). \quad (4.11b)$$

Equation (4.9) can be simplified to the one-dimensional Eqs. (4.10) and (4.10'). This tells us immediately that for large values of ΔR , at intermediate times the eigenvalues are given approximately by

$$K_n \approx \left(n + \frac{1}{2}\right) \pi \text{ for } K_n \ll \Delta R, \quad (4.12)$$

where n is an integer, while at larger K_n (shorter times) the eigenvalues shift to

$$K_n \approx n \pi \text{ for } K_n \gg \Delta R. \quad (4.13)$$

In both regimes, the eigenvalues have a spacing of $(K_{n+1} - K_n) \approx \pi$, with a transition regime, where, because of smoothness, the spacing is somewhat shorter or larger, but never smaller than $\pi/2$ or larger than $3\pi/2$.

We have, therefore, defined the interval in which to look for the eigenvalue K_{n+1} iteratively by $(K_n + \pi/2, K_n + 3\pi/2)$. In this way it is impossible to overlook a single eigenvalue. We have found that for the determination of K_3 this method is already sufficient. Due to the gap between K_1 and K_2 , only for the determination of the second eigenvalue the intervals $(K_1 + \pi/2, K_1 + 3\pi/2)$, $(K_1 + 3\pi/2, K_1 + 5\pi/2)$, etc. have to be scanned successively, until K_2 is found.

The amplitudes a_n and b_n are finally gotten from Eq. (4.6),

$$a_n = -\frac{1}{N} Y_{d/2}(k_n R_1), \quad (4.14a)$$

$$b_n = \frac{1}{N} J_{d/2}(k_n R_1), \quad (4.14b)$$

where we have used, for simpler notation, the shell radii R_0 and R_1 , together with k_n again. The normalization term N in Eqs. (4.14) is gotten from the normalization condition for the eigenfunctions, Eq. (4.3). Using the abbreviations $(m, n = 0, 1)$,

$$J_{mn} = J_{d/2-m}(k_n R_m), \quad (4.15a)$$

$$Y_{mn} = Y_{d/2-m}(k_n R_m), \quad (4.15b)$$

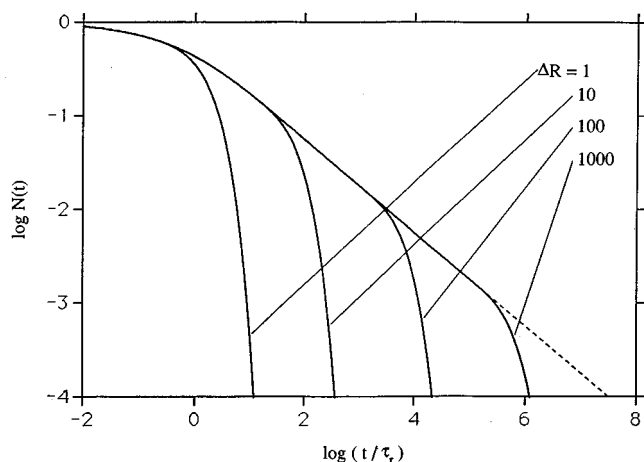


FIG. 3. $N(t)$ vs t for $d=1$; ΔR as indicated; the dashed line is the behavior predicted by Eq. (3.11).

this normalization term can be cast into the form

$$N = \frac{1}{2} R_1^2 (Y_{01} J_{11} - J_{01} Y_{11}) + \frac{1}{2} R_0^2 [(Y_{01} J_{10} - J_{01} Y_{10})^2 - (Y_{01} J_{00} - J_{01} Y_{00})(Y_{01} J_{10} - J_{01} Y_{10})]. \quad (4.16)$$

The numerical method we have chosen here is different from other viable numerical approaches like space-discretization, followed by either generalized moment expansion³⁸ or an eigenvalue analysis,^{9,10} or from short-time approaches like Chebyshev propagation.³⁹ We see some advantage in working with the eigenfunction expansion of the original reaction-diffusion operator in its infinite-dimensional Hilbert space of functions. For example, it is not necessary to check whether a discretization employed is fine enough to catch all phenomena correctly. Instead, the above algorithm gives successively *all* numerically exact eigenvalues of the operator, starting from the lowest one, i.e., from the longest time scale. Therefore, the dynamics is obtained correctly down to the time scale corresponding to the highest eigenvalue included. For the cases of interest, this number can be quite large, i.e., several thousand.

B. Results

Figure 3 shows results for the one-dimensional case with finite boundary. After an initial transient, which ends at about $t \approx 1$, one can see clearly the algebraic decay with $t^{-1/2}$, which is predicted by Eqs. (3.11) and (3.12) for the case of an infinite boundary. Both regimes are described correctly by Eq. (3.11). With a finite boundary, the algebraic decay ends at some finite time and changes into a single-exponential cutoff. The time scale of this cutoff grows quadratically with ΔR , and can be described by the generalized moment approximation; see Sec. V below.

In Fig. 4 results are shown for a typical situation in three dimensions for fixed large values of X and ΔR . It still shows the initial transient, followed by an intermediate algebraic decay. Both can be described by the one-dimensional result,

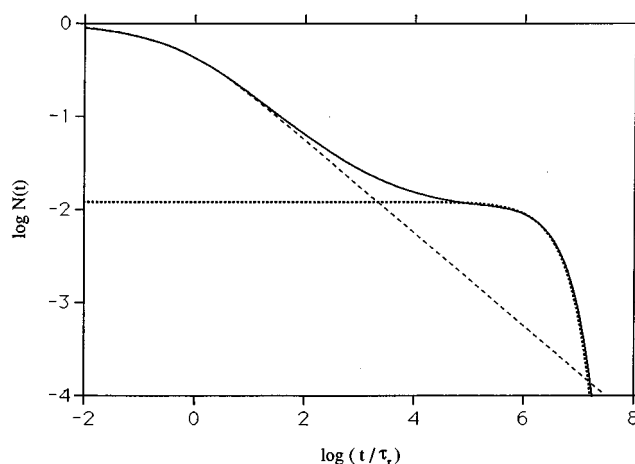


FIG. 4. $N(t)$ vs t for $d=3$, $\Delta R=1000$, and $X=10$; the dashed line is the behavior predicted by Eq. (3.11); the dotted line is the single-exponential long-time fit, Eq. (5.10).

Eq. (3.11). However, here a new feature emerges. At some time τ^* , the algebraic decay levels off to a behavior that looks like a plateau in the double-logarithmic plots we use to present our data, i.e., the data appear to stabilize at a value $N(t) \approx N_{\text{plateau}}$. This plateau is essentially the single-exponential long-time decay. Since there emerges a large gap between the lowest and the second-lowest eigenvalue—see the discussion in Sec. IV D below—this gap represents itself as a plateau in that representation of the data.

Figures 5(a) and 5(b) show how the relationship between algebraic decay and plateau regime depends on the parameters ΔR and X . As Fig. 5(a) clearly demonstrates, large values of the parameter X are responsible for the plateau regime. Increasing values of X lead to an increasing length of the plateau regime, concomitant with an increasing value of $N(t)$ at the plateau. Conversely, ΔR controls mainly the position in time of the plateau regime. Figure 5(b) demonstrates that the form of the plateau regime is more or less invariant against variations of the value of ΔR , as long as the plateau regime is still recognizable. An increase of ΔR mainly results in a shift of the plateau regime to longer times.

Figure 6 finally shows the dependence of the plateau regime on the space dimension. Starting with $d=2$ a deviation from the one-dimensional algebraic $t^{-1/2}$ decay occurs, which appears as a stabilization of the value of $N(t)$ during some time interval, the plateau. This effect becomes more pronounced as the space dimension increases. The time for the onset of the plateau decreases, while the cutoff time increases with d , resulting in an increasing length of the plateau at increasing values of N_{plateau} . The latter result is in accord with the different forms of the Polya escape results, which predict an increase of the escape probability with d . It will be shown in Sec. V below that, indeed, the plateau value converges to the Polya value for $\Delta R \rightarrow \infty$.

The case of $d=2$ requires some more discussion. As can be seen in Fig. 7 and in Fig. 8, there is a clear deviation from the one-dimensional behavior. However, whether this new

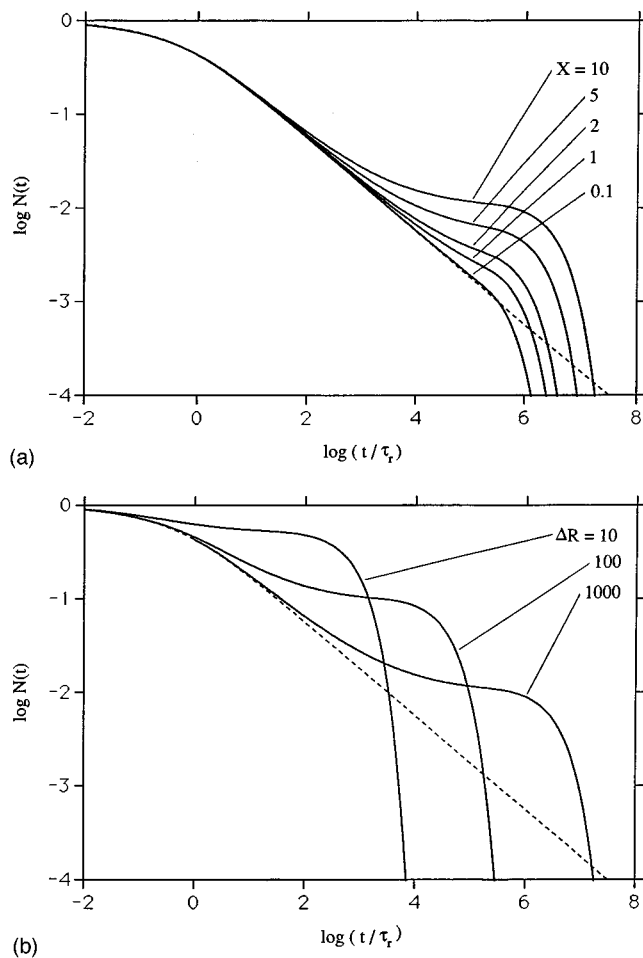


FIG. 5. $N(t)$ vs t for $d=3$, (a) $\Delta R=1000$ and X as indicated, (b) $X=10$ and ΔR as indicated; the dashed line is the behavior predicted by Eq. (3.11).

behavior may be called a plateau—as it clearly can in $d > 2$ —or not may be seen as a question of convention.⁴⁰ Strictly speaking, there is no plateau in the limit $\Delta R \rightarrow \infty$ since the plateau value N_{plateau} vanishes in that limit; see also Sec. V below. However, for finite values of ΔR , the amplitude of the exponential cutoff is nonzero, concomitant with an increasing gap between the lowest and the second lowest eigen-

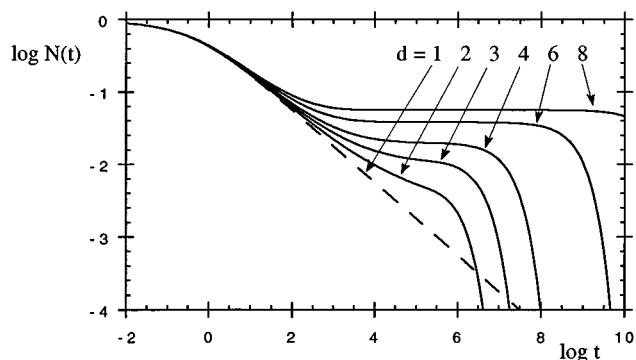


FIG. 6. $N(t)$ vs t for $\Delta R=1000$ and $X=10$, and d as indicated; the dashed line is the behavior predicted by Eq. (3.11).

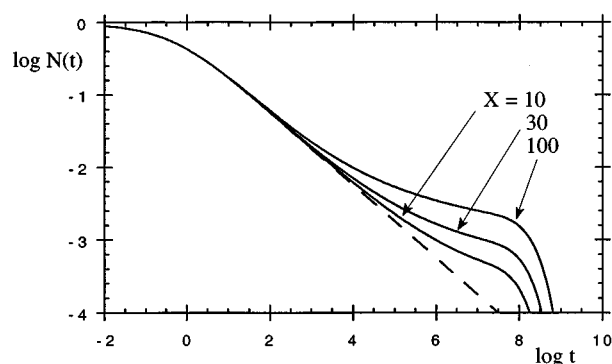


FIG. 7. $N(t)$ vs t for $d=2$, $\Delta R=1000$, and X as indicated.

value, see Sec. IV D below. We interpret the developing structure in $N(t)$ in $d=2$ as a plateau, although it can be considered *marginal* since it vanishes in the limit $\Delta R \rightarrow \infty$.

C. Dimension-independence of decay at short and intermediate times

Our numerical results, reported in Ref. 13 and the previous sections of this paper, have indicated that the behavior of both the transient short-time and the intermediate-time algebraic decay regimes are both independent of dimension. In Sec. III C it was further claimed that placing the initial position of the diffusing particle on the inner reacting boundary was sufficient to produce the dimension-independent $t^{-1/2}$ decay at intermediate times. In this section we demonstrate this assertion analytically by direct examination of the eigenvalue equations in the short- and intermediate-time domains. We consider the cases of both a reflecting and an absorbing outer boundary. For both cases we derive the $t^{-1/2}$ decay at intermediate times; this corresponds to our assertion that it is the proximity of the particle's initial position to the inner boundary that drives this decay, and the outer boundary plays no role in this portion of the falloff.

The arguments in this section are purely mathematical; alternative derivations and accompanying physical explanations for the observed dimension-independence are given in Secs. III C and V.

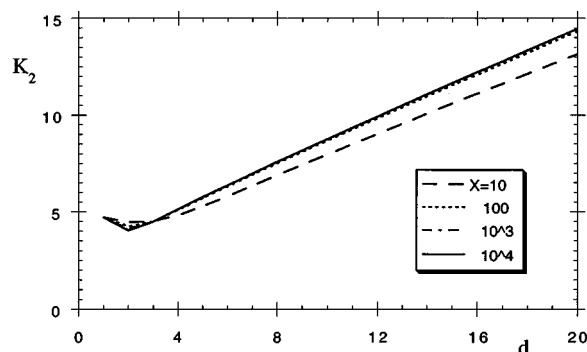


FIG. 8. K_2 vs d for $X=10, 10^2, 10^3, 10^4$.

We study first the general d -dimensional reaction-diffusion model with reflecting outer boundary [Eqs. (2.8)–(2.10a)]. The solution of the diffusion equation in d dimensions, written as an eigenfunction expansion, and subject to initial condition Eq. (2.7), is given by Eqs. (4.1) and (4.3),

$$p(r,t) = \sum_n \exp(-k_n^2 t) r^{1-d/2} [a_n J_{1-d/2}(k_n r) + b_n Y_{1-d/2}(k_n r)] R_0^{1-d/2} [a_n J_{1-d/2}(k_n R_0) + b_n Y_{1-d/2}(k_n R_0)], \quad (4.18)$$

where as usual we use dimensionless space and time variables. We also replace r_0 in Eq. (2.7) with R_0 because we use here the initial condition that the particle starts at the inner reactive boundary.

We now consider an outer reflecting boundary at R_1 in addition to the inner reactive boundary at R_0 . The inner boundary condition is described by Eq. (2.9) and the outer by Eq. (2.10a). The resulting eigenvalue equation is given by Eq. (4.9).

We now introduce our main approximation, namely that $k_n R_0 \gg 1$. Physically, this amounts to looking at times short compared to those needed for ligands to diffuse very far into the region between the two boundaries, which corresponds to the short and intermediate times that we are interested in. Specifically, the algebraic decay regime comes about from interaction with the inner boundary, as already stated; the outer boundary is responsible for the position of the plateau, related to the previously discussed Polya limit, and the subsequent exponential decay of $N(t)$. Because $R_1 > R_0$, our condition automatically implies that $k_n R_1 \gg 1$. Furthermore, because we have already seen that the situation of biological and physical interest is where $\Delta R = (R_1 - R_0)/l_r$ is large compared to one, we confine ourselves to the further condition that $k_n \Delta R \gg 1$. These are our only approximations, which result in the simplified eigenvalue Eq. (4.10').

The error in Eq. (4.10') is of order $1/k_n R_0$. As discussed in Sec. IV A, numerical analysis indicates that in all cases Eq. (4.10') becomes an accurate expression for the eigenvalues after the first three or four.

Using this and results for a_n and b_n from Sec. IV A, we find

$$R_0^{d-1} p(R_0, t) = (2/\Delta R) \sum_{n=0}^{\infty} e^{-k_n^2 t} \cos^2(k_n \Delta R). \quad (4.19)$$

In Eq. (4.19) we let the sum run from $n=0$, even though the approximations involved break down for the first few eigenvalues. However, as long as we restrict ourselves to times short compared to $\tau_r r_0/l_r$, the error involved will be exponentially small.

The left-hand side of Eq. (4.19) is equal to $-(d/dt)N(t)$, as discussed in Sec. II. Because Eq. (4.10') and therefore Eq. (4.19) are independent of dimension, we have already shown that for times short compared to $\tau_r r_0/l_r$, the time decay of $N(t)$ is independent of dimension. We can go further, however, and derive the $t^{-1/2}$ decay at intermediate times.

We already have the restriction that $k_n \Delta R \gg 1$. Because we are also restricted to the biologically relevant case where $\Delta R \gg 1$, k_n itself can be small or large compared to one. Smaller k_n 's correspond to longer times, and in particular k_n small compared to one (but large compared to $1/\Delta R$) corresponds to the intermediate time regime, where we expect to see the algebraic decay. We can then use Eq. (4.12) for k_n small compared to unity, and for larger k_n (shorter times) we use Eq. (4.13).

Equation (4.19) can then be rewritten, using Eq. (4.10'), as

$$-\frac{d}{dt} N(t) = (2/\Delta R) \sum_{n=0}^{\infty} e^{-k_n^2 t} k_n^2 \sin^2(k_n \Delta R). \quad (4.20)$$

At intermediate times, when Eq. (4.12) holds, $\sin^2(k_n \Delta R) \approx 1$. Substituting Eq. (4.12) into Eq. (4.20), we find that the sum on the right-hand side now depends on n as $\sum n^2 e^{-n^2 t}$ (with the n 's now half-integers). Because the terms in the summand are closely spaced, we can convert the sum to an integral, and immediately scale out the t -dependence to find

$$-\frac{d}{dt} N(t) \sim t^{-3/2} \quad (4.21)$$

which gives the $t^{-1/2}$ decay.

The previous discussion used a reflecting boundary at R_1 . Even though R_1 must therefore enter the eigenvalue equations, we expect physically that the precise nature of the outer boundary condition cannot affect the physics at short and intermediate times. That this is the case can be seen by repeating the previous discussion with only one change; we replace the reflecting boundary at R_1 with an absorbing one. These two outer boundary conditions represent diametrically opposite situations. The new outer boundary condition is then

$$p(R_1, t) = 0. \quad (4.22)$$

The eigenvalue equation Eq. (4.9) is replaced by

$$k_n = \frac{J_{1-d/2}(k_n R_1) Y_{1-d/2}(k_n R_0) - J_{1-d/2}(k_n R_0) Y_{1-d/2}(k_n R_1)}{J_{1-d/2}(k_n R_1) Y_{-d/2}(k_n R_0) - J_{-d/2}(k_n R_0) Y_{1-d/2}(k_n R_1)}. \quad (4.23)$$

Using the same approximations as before gives

$$\tan(k_n \Delta R) = -k_n. \quad (4.24)$$

The arguments used for the reflecting outer boundary can now be repeated; we now find that

$$R_0^{d-1} p(R_0, t) = (2/\Delta R) \sum_{n=0}^{\infty} e^{-k_n^2 t} \sin^2(k_n \Delta R). \quad (4.25)$$

Using the new eigenvalue equation Eq. (4.24), we find

$$R_0^{d-1} p(R_0, t) = (2/\Delta R) \sum_{n=0}^{\infty} k_n^2 e^{-k_n^2 t} \cos^2(k_n \Delta R). \quad (4.26)$$

Note that the new eigenvalues, relative to those for the reflecting outer boundary, are simply shifted by $\pi/2$; also that the difference $k_{n+1} - k_n$ between adjacent eigenvalues is unchanged. Equation (4.26) then becomes identical [up to $O(1/k_n \Delta R)$] to Eq. (4.19). This is not the end of the story, however, because $-(d/dt)N(t)$ is no longer equal to the left-hand side of Eq. (4.26). This is because the outer absorbing boundary condition implies no incoming flux of particles at the outer boundary. Because we are restricting ourselves to times much shorter than those required for particles to diffuse to the outer boundary, however, this term makes a negligible contribution to $N(t)$ [in fact, its contribution is of $O(1/k_n R_1)$] and our earlier conclusions remain unchanged.

We have shown, for short and intermediate times, that when the initial position of the diffusing particle is on the inner reactive boundary, the short- and intermediate-time behavior of $N(t)$ is independent of dimension, and we have derived the universal $t^{-1/2}$ algebraic decay at intermediate times. Our analysis also supports conclusions generated by our numerical studies, in particular that the condition $\Delta R \gg 1$ is necessary for the algebraic decay to be observed at all (if the outer boundary is too close to the inner boundary, exponential decay sets in almost immediately).

A second conclusion can be drawn. In order to derive the $t^{-1/2}$ algebraic decay, we needed that a subset of the relevant k_n 's be small compared to unity. Our starting condition was that $k_n R_0 \gg 1$. If R_0 itself is not too small, this is perfectly consistent with $k_n < 1$. However, for values of R_0 (in units of l_r) which are too small, the two conditions are incompatible, and no $t^{-1/2}$ decay arises from our calculations. But this conclusion is consistent with our other condition (see Sec. V) that the value of X not be too large.¹³ Our analytical results, therefore, not only support our numerical conclusions but also shed some light on their physical origins.

D. Eigenvalues and the plateau

Finally, we want to investigate what a closer look at the eigenfunction expansion can tell us about the plateau regime that we observed in our numerical results.

The existence of a plateau regime in a double logarithmic plot, like the one in Figs. 3–7, is an indication that there is a considerable gap in the values of the time constants of the eigenfunction expansion. In other words, if the eigenvalues are ordered, $k_1 < k_2 < k_3 \dots$, then there is an n , so that $k_n \ll k_{n+1}$ holds. Since the final decay of $N(t)$ is single-exponential, which is particularly well illustrated by the single-exponential long-time approximation in Fig. 4, see also Sec. V below, this gap should appear between k_1 and k_2 .

In order to investigate this in more detail, we will analyze the behavior of the system size-scaled eigenvalues K_n , Eq. (4.8), for $n=1,2$ on X in the limit $\Delta R \rightarrow \infty$. It is reasonable to employ this limit, since, as the results presented above show, a plateau regime appears only for large system size, and, as Fig. 5(b) demonstrates, the length of the plateau in a logarithmic plot is practically independent of ΔR . An additional advantage is that the eigenvalue equation (4.9) simplifies to

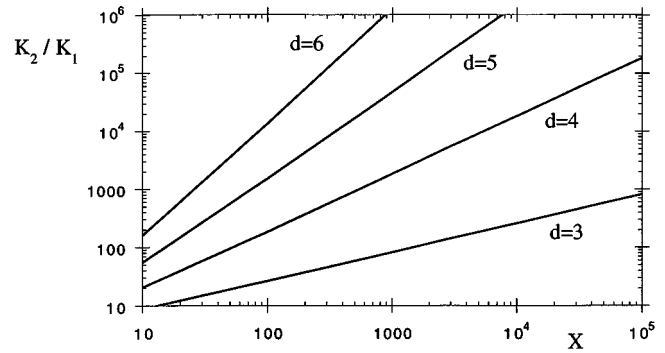


FIG. 9. K_2/K_1 vs X for $d > 2$, as indicated; note that the lines have a slope of $(d-2)/2$.

$$J_{1-d/2} \left(K_n \frac{1}{X} \right) Y_{-d/2} \left[K_n \frac{X}{(1+X)} \right] - J_{-d/2} \left[K_n \frac{X}{(1+X)} \right] Y_{1-d/2} \left(K_n \frac{1}{X} \right) = 0. \quad (4.27)$$

The ratio K_2/K_1 is a direct measure of the length of the plateau in a double-logarithmic representation. Figure 8 demonstrates that K_2 becomes practically independent of X for large values of X , and increases almost linearly with d . K_1 , on the other hand, depends strongly on both X and d , decreasing with both. Because of the weak dependence of K_2 on X , we refrain from presenting the data for K_1 directly, but, rather, show how the ratio K_2/K_1 depends on X and d in Figs. 9 and 10. Figure 9 demonstrates that the ratio K_2/K_1 grows with X according to a power law,

$$K_2/K_1 \propto X^{(d-2)/2}. \quad (4.28)$$

Interestingly, $(d-2)/2$ is the same exponent with which $N(t)$ decays to its Polya limit in the semi-infinite system, see Sec. III C. In $2d$ the ratio depends only logarithmically on X ,

$$K_2/K_1 \propto \sqrt{\ln X}, \quad (4.29)$$

as Fig. 10 shows.

Since the ratio K_2/K_1 grows without bounds with X for all dimensions $d > 1$, it is clear that a plateau will emerge for

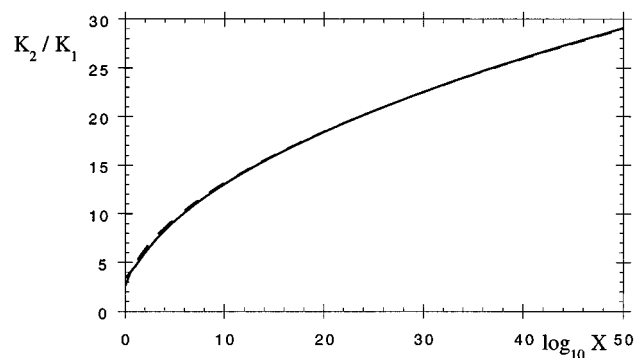


FIG. 10. K_2/K_1 vs X for $d=2$; the dashed fit is $4.1 \sqrt{\log(0.41+X)}$.

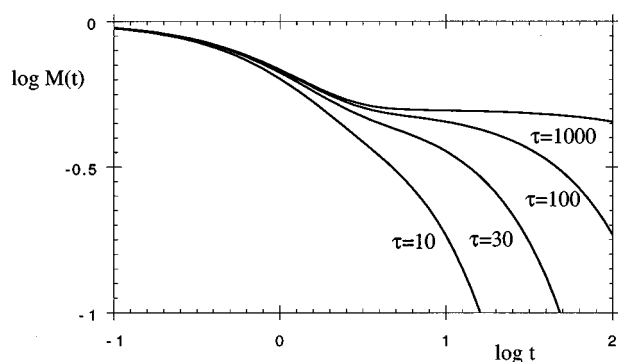


FIG. 11. Test function $M(t)$, Eq. (4.30), vs t , τ as indicated.

sufficiently large values of X . It remains to be determined what such a sufficiently large value of X is, depending on dimension. For that purpose let us consider a simple test function, a sum of two exponentials,

$$M(t) = \frac{1}{2} (e^{-t} + e^{-t/\tau}), \quad (4.30)$$

where τ is a measure of the ratio of the two time constants. Figure 11 shows the behavior of $M(t)$ in a double logarithmic plot for various values of τ . In $1d$ the ratio of eigenvalues in the limit $\Delta R \rightarrow \infty$ is $K_2/K_1 = 3$. Since $(K_2/K_1)^2 = \tau_1/\tau_2$, this value corresponds approximately to the curve for $\tau = 10$ in Fig. 11, clearly no plateau. However, it can be seen that a plateau already begins to emerge in the range $\tau \approx 30$ – 100 . Therefore, a value of $(K_2/K_1)^2 \approx 6$ – 10 can be considered a lower threshold for the ratio of the lowest eigenvalues in order to produce a recognizable plateau regime. From Fig. 9 it can be seen that $X \approx 10$ is sufficient in $3d$, and for larger dimensions the threshold values for X are still lower. In $2d$, however, due to the logarithmic dependence of K_2/K_1 on X , the lowest values of X necessary to produce a recognizable plateau are in the range $X \approx 100$ – 1000 .

V. GENERALIZED MOMENT ANALYSIS

The method of generalized moment expansion^{26,27,28,41,38} allows an analytical analysis of the approximate long-time behavior of $N(t)$ for finite ΔR . In particular, it provides a possibility to obtain approximate analytical expressions for the time constant of the exponential cutoff—corresponding to the lowest eigenvalue—and for the value of $N(t)$ in the plateau regime. In the following we give a short review of the basic ideas.

The long time (or low frequency) moments of $N(t)$ are defined by

$$\mu_{-n} = (n-1)! \int_0^\infty t^{n-1} N(t) dt. \quad (5.1)$$

They can be written formally as matrix elements of the inverse of the adjoint stochastic operator $\nabla_{r_0}^2$ introduced in Sec. III C,²⁸

$$\mu_{-n} = [-\nabla_{r_0}^2]^{-n} \mathbf{1} = \langle \delta(r-r_0) [-\nabla_r^2]^{-n} \mathbf{1} \rangle, \quad (5.2)$$

where $\mathbf{1}$ denotes the constant function of value 1, $\langle \rangle$ denotes the integral over r from R_0 to R_1 and has the properties of an inner product on the space of functions, and the delta function comes from the initial condition, Eq. (2.2). ∇_r^2 can be cast into the somewhat more convenient form

$$\nabla_r^2 = \frac{1}{r^{d-1}} \frac{d}{dr} r^{d-1} \frac{d}{dr}, \quad (5.3)$$

supplied with the adjoint boundary conditions,²⁶

$$\left. \frac{d}{dr} f(r) \right|_{r=R_0} = f(R_0), \quad (5.4a)$$

$$\left. \frac{d}{dr} f(r) \right|_{r=R_1} = 0, \quad (5.4b)$$

that any function $f(r)$ on which ∇_r^2 operates has to obey.

It is useful to define the auxiliary functions

$$\mu_{-n}(r) = [-\nabla_r^2]^{-n} \mathbf{1} \quad (5.5)$$

from which we can obtain the desired moments by evaluating them at $r=R_0$. For $n=1,2,\dots$, these functions can be determined iteratively via the set of equations

$$\nabla_r^2 \mu_{-n}(r) = -\mu_{-(n-1)}(r) \quad (5.6)$$

using

$$\mu_0(r) = 1 \quad (5.7)$$

as the starting function. The general solution of Eq. (5.6) under the boundary conditions (5.4) is

$$\begin{aligned} \mu_{-n}(r) = & R_0^{(1-d)} \int_{R_0}^{R_1} r_1^{d-1} \mu_{-(n-1)}(r_1) dr_1 \\ & + \int_r^{R_1} r_1^{1-d} \int_{R_0}^{r_1} r_2^{d-1} \mu_{-(n-1)}(r_2) dr_2 dr_1. \end{aligned} \quad (5.8)$$

The evaluation of the integrals in Eq. (5.8) is tedious but straightforward. We give here the results for μ_{-1} and μ_{-2} ,

$$\mu_{-1} = \Delta R (Y^d - 1) / Xd \quad (5.9a)$$

$$\begin{aligned} \mu_{-2} = & \{ \Delta R^2 X (Y^d - 1)^2 (d^2 - 4) + \Delta R^3 [2 - d + Y^d (d^2 - 4) \\ & - Y^{2+d} d^2 + Y^{2d} (d+2)] \} / \{ X^3 d^2 (d^2 - 4) \}, \end{aligned} \quad (5.9b)$$

where the abbreviation $Y = (1+X)$ was used.

Based on the generalized moments of a relaxational dynamical observable $N(t)$, one can define single-, multi-, and nonexponential approximations that reproduce a specified number of those moments.^{28,42} Of particular interest in our case is a single-exponential approximation that reproduces the moments μ_{-1} and μ_{-2} of the exact function $N(t)$. It is easy to see that such an approximation has the form

$$N_{\text{long}}(t) = q_l \exp(-t/\tau_l), \quad (5.10)$$

with the time constant τ_l given by

$$\tau_l = \mu_{-2} / \mu_{-1}, \quad (5.11)$$

and the amplitude q_l given by

$$q_l = \mu_{-1}^2 / \mu_{-2}. \quad (5.12)$$

The time constant τ_l is an approximation to the time constant of the exponential cutoff, i.e., the inverse of the lowest eigenvalue. It can be shown that the ratio of successive moments $\mu_{-n} / \mu_{-(n+1)}$ converges to the lowest eigenvalue.⁴³ The inverse of the first possible ratio is the well-known mean first passage time⁴⁴⁻⁴⁶

$$\tau_{\text{MFPT}} = \mu_{-1} / \mu_0 = \mu_{-1}, \quad (5.13)$$

and is used quite often as an approximation to the inverse of the lowest eigenvalue.⁴⁵ But when $N(t)$ exhibits nonexponential behavior—as in our case—the mean first passage time is not a good estimate of the exponential cutoff. However, it turns out that the second ratio, which determines τ_l , already provides an acceptable approximation in most cases, see Fig. 4.

The quantity q_l is an approximation to the contribution of the exponential cutoff to the overall decay of $N(t)$ and, as such, it provides an estimate of the plateau value at which $N(t)$ stabilizes, before it finally decays exponentially. q_l also provides a bridge to the semi-infinite system results derived in Sec. III. In the limit $R_1 \rightarrow \infty$ the approximation (5.10) should still exhibit some aspects of the behavior of $N(t)$. Indeed, in that limit $\tau_l \rightarrow \infty$, and q_l becomes the escape probability of Polya's theorem

$$\lim_{R_1 \rightarrow \infty} q_l = \begin{cases} 0 & d \leq 2 \\ \frac{d-2}{R_0+d-2} & d \geq 3 \end{cases}; \quad (5.14)$$

compare Eq. (3.34). For $d=1$, the amplitude q_l vanishes as $q_l \propto \Delta R^{-1}$, whereas for $d=2$ it vanishes only logarithmically,

$$q_l \propto \frac{1}{R_0 \ln(R_1)}. \quad (5.15)$$

This is another indication of the marginal behavior in $2d$. It is quite surprising that a simple single-exponential approximation like Eq. (5.10) is already able to reproduce such a complicated limiting behavior.

These results on the exponential long-time cutoff now allow us to analyze the algebraic and the plateau regime from a point of view different from the eigenfunction expansion approach employed in Secs. IV C and IV D.

One necessary condition for the algebraic regime (and, possibly, the plateau) to be present at all is that the cutoff time scale τ_l is much larger than the time for the initial transient, which is of $O(1)$. For fixed values of X and ΔR large $\tau_l \propto \Delta R^2$ holds in all dimensions. For fixed values of ΔR and X large $\tau_l \propto X^{d-1}$ holds in $d > 1$. Asymptotically for $\Delta R \rightarrow \infty$, however, $\tau_l / \Delta R^2 \propto X^{d-2}$ holds in $d > 2$, while $\tau_l / \Delta R^2 \propto \ln(X)$ holds in $2d$. Therefore, the condition $\tau_l \gg 1$ can always be met by sufficiently large values of X and ΔR . Note that, as will be discussed in more detail below, $\tau_l / \Delta R^2$ exhibits the same asymptotic properties as $(K_2 / K_1)^2$, introduced in Sec. IV D above.

A crossover time τ^* from the algebraic $t^{-1/2}$ -decay to the plateau regime can be estimated through the relation

$$N_{1d}(\tau^*) \approx q_l, \quad (5.16)$$

giving rise to

$$\tau^* \approx \frac{1}{\pi q_l}. \quad (5.17)$$

The other condition for the existence of the algebraic regime is that this crossover time τ^* is also much larger than the initial transient time.

Since τ^* is proportional to the square of the inverse of q_l , we can use our knowledge of the asymptotic behavior of q_l , see Eq. (5.14), for an analysis of the behavior of τ^* . For $d > 2$ we find from the Polya limit that τ^* assumes the limiting value, $\tau^* \rightarrow [(R_0 + d - 2)^2 / \pi(d - 2)^2]$ for $R_1 \rightarrow \infty$. Therefore, in order that $\tau^* \gg 1$ also large values of R_0 are necessary in this limit. A large Polya value $N(\infty)$ simply reduces the length of the algebraic regime. In $2d$ q_l vanishes for $R_1 \rightarrow \infty$, although logarithmically, thereby guaranteeing that $\tau^* \rightarrow \infty$, too, fulfilling the necessary condition for an algebraic regime to be present in this limit for *all* values of R_0 . In $1d$ the quantity τ^* does not make any sense since we know that only τ_l controls the algebraic regime here. We note, however, that also here $\tau^* \gg 1$ for $\Delta R \gg 1$ holds.

Since we know from Sec. IV that ΔR and X regulate the algebraic and the plateau regime antagonistically, it is interesting to also analyze the dependence of τ^* on these quantities. Surprisingly, we find no qualitative difference between $d > 2$ and $d = 2$ here. For fixed values of X and ΔR large $\tau^* \propto \Delta R^2$, i.e., τ^* exhibits the same behavior τ_l . Therefore, large values of ΔR increase the length of the algebraic regime, as Fig. 5(b) demonstrated. However, for fixed values of ΔR and X large we find $\tau^* \rightarrow \pi^{-1}$. In other words, τ^* decreases with increasing X , thereby shortening the range of the algebraic regime, letting it vanish altogether for $X \rightarrow \infty$.

These different results for $R_1 \rightarrow \infty$ on the one hand, and for $\Delta R \rightarrow \infty$ with X fixed and $X \rightarrow \infty$ with ΔR fixed, on the other hand, may appear surprising. However, one has to note the limits are not interchangeable. $R_1 \rightarrow \infty$ corresponds to a combined limit $\Delta R \rightarrow \infty$ together with $X \rightarrow \infty$. Note that the parameter X , which describes the ratio of the thickness of the d -dimensional shell to its inner radius of curvature, controls the effective dimensionality of the diffusion shell. $X \rightarrow 0$ is the limit of an extremely thin diffusion shell and corresponds, therefore, to an effectively $1d$ situation. $X \rightarrow \infty$, on the other hand, corresponds to a d -dimensional sphere of radius $R_1 \rightarrow \infty$ with an absorptive point in the center, i.e., $R_0 \rightarrow 0$. Equation (5.15) shows that in this combined limit q_l can remain finite also in $2d$.

In terms of the above defined quantities, a necessary condition for the plateau regime to be clearly visible is $\tau_l \gg \tau^*$, else the algebraic regime will cross over directly to the exponential tail. Therefore, the ratio

$$\frac{\tau_l}{\tau^*} = \frac{\mu_{-1}^3}{\mu_{-2}} \quad (5.18)$$

controls the existence of the plateau regime. This function grows monotonically with ΔR , X , and d , and its asymptotic properties follow directly from the asymptotic properties of τ_l and τ^* discussed above. It is instructive to look at $d=1$ first. Here we find $\tau_l/\tau^* \rightarrow 3\pi$ in the limit $\Delta R \rightarrow \infty$. Since there is no plateau in $1d$, this value gives a lower limit for τ_l/τ^* in order for a plateau to exist. The difference between one and higher dimensions is that for $d>1$ the ratio τ_l/τ^* becomes infinite for $X \rightarrow \infty$, even for finite ΔR , whereas in one dimension τ_l/τ^* always remains small. We conclude, therefore, that a plateau regime will be seen in dimensions two and higher, provided that the values of X and ΔR are large enough. This conclusion is also supported by the numerical results presented in Sec. IV.

One has to note that the behavior of the ratio τ_l/τ^* is different from the ratio of the lowest eigenvalues, K_2/K_1 , analyzed in Sec. IV D. Since K_2 is practically constant for large X and $1/\tau_l$ is an estimate for K_2^2 , the behavior of K_2/K_1 is similar to that of $\sqrt{\tau_l}$, presented above; $K_2/K_1 \propto X^{(d-2)/2}$ for $d>2$ and $K_2/K_1 \propto \sqrt{\ln(X)}$ in $2d$. This behavior was also obtained in the numerical results of Sec. IV D. Equation (5.18), on the other hand, exhibits $\tau_l/\tau^* \propto X^d$ for $d>2$ and $\tau_l/\tau^* \propto X^2/\ln(X)$ for $2d$. The reason for this discrepancy is that τ^* is actually an estimate for the center of the transition area between the algebraic regime and the plateau regime, while K_2/K_1 is an estimate for the range of the plateau regime only. The different behavior of both ratios demonstrate that, together with the plateau regime, also the range of the transition regime grows with X .

VI. GENERIC DESCRIPTION OF MACROSCOPIC PROTEIN FLUCTUATIONS

At physiological temperatures, proteins fluctuate strongly between different microscopic conformations.^{47,48,49} On a macroscopic level, these microscopic fluctuations manifest themselves as fluctuations between protein states of different functionality. One simple, well-known example is a protein acting as a passive ion channel which can be either in an open or a closed state.^{50,51} Other examples are fluctuations of transport proteins between states of different binding activity for the ligand,^{23,6} or fluctuations of catalytic proteins between states of different catalytic effectivity. We will advocate here a new generic—albeit abstract—view for the description of these macroscopic manifestations of microscopic conformational fluctuations.

Proteins are an example of complex systems with a high-dimensional state space.⁵² This space of microscopic conformations can be partitioned into sets corresponding to the different macroscopic protein states. Usually, several microscopic conformations that are close to each other in state space will belong to the same macroscopic state and will form a—more or less extended—individual patch. All patches that belong to one particular macroscopic state then make up one partition set; see Fig. 12. There are several relevant topologies for the respective structures of the partition regions in that high-dimensional state space; one or several of them may percolate throughout the entire state space,

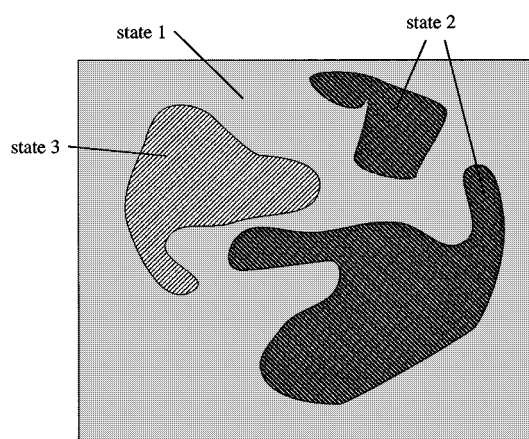


FIG. 12. Sketch of the state space partitioning.

but not the others, or even all of them may percolate. Note that, due to the high dimensionality of the state space, independent percolation of different partitions is possible.⁵³ However, having neither percolate requires special geometries and is unlikely to be encountered.⁵⁴

Thermal fluctuations can—in general—be modeled successfully as a random walk in some state space.^{44–46} Conformational fluctuations of proteins, particularly at physiological temperatures, are no exception to that. Fluctuations of the macroscopic state of a protein arise in this picture from the random walk leaving a patch corresponding to one macrostate, and entering the patch of another macrostate. During the time the random walk stays in that patch the protein stays in that macrostate, until it leaves the patch again, either to enter the one it came from or to enter another, see also Fig. 12. We will call this approach the *random walk on state space partitions* picture of macroscopic fluctuations.

Due to the complicated interactions involved in a strongly heterogeneous system like a protein, the random walk in protein state space has to be viewed as one on a very rugged potential surface.^{55,56} Particularly in the low temperature regime, this ruggedness imposes strong limitations on the parts of state space that are accessible at all, a feature known as “broken ergodicity.”^{57,58} Although there has been considerable work on stochastic processes on rugged potentials, the properties of macroscopic fluctuations due to rugged potential random walks on partitions is completely unknown up to now. Nevertheless, they could probably give very interesting new insights into the low-temperature behavior of glasses and of proteins.

Here, however, we will be concerned with the high temperature regime. In this regime, random walks on rugged potentials can be viewed on macroscopic length scales as free diffusion with some suitably renormalized diffusion coefficient.^{59,60} It is also known that, e.g., Mössbauer data on protein fluctuations can be described successfully using an effective temperature-dependent diffusion coefficient in a smooth, slowly-varying potential.^{61,38} We will, therefore, assume in the following that the random walk in the protein conformational state space can be described in a first approximation as free diffusion.

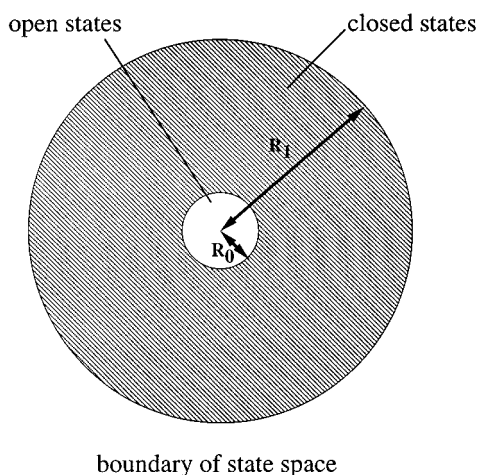


FIG. 13. Sketch of the state space partitioning for the ion channel opening and closing fluctuations.

The open-state/closed-state fluctuations of passive ion channel proteins are a very suitable candidate for applying the scheme that we sketched above. In this case there is a simple, natural partitioning of state space, namely the open and closed states. In this approach, a channel that switches, e.g., from the open to the closed state can be thought of as crossing the boundary from a region of open-state configurations to a region of closed-state configurations. On the other hand, there exists already a vast array of experimental literature on the fluctuation properties of these channel proteins; see e.g. Ref. 62, and references therein. Since single-channel fluctuations can be monitored individually using the patch clamp technique,⁶³ opening and closing times are readily accessible for a statistical analysis. In particular, the distribution of closing times, $P_{\text{closed}}(t)$, is often observed to exhibit an algebraic regime with a $t^{-3/2}$ power law in many ion channel proteins.^{64–67}

Although the mutual topology of the open and closed state partitions is not known, i.e., it is not known whether only one or both of them percolate, it is reasonable to assume that there is a much smaller number of open states than of closed states, since open channels require a much more restricted arrangement of atoms. We can, therefore, assume that the closed state partitions result in one or more isolated open patches. The existence of several different patches of isolated open states in state space, separated from each other by areas of closed states, would correspond to a situation where several, structurally very different, open channel conformation classes exist. We will assume in the following that this is not the case, and that a single patch of open states exists in state space, which is surrounded by closed states. Assuming spherical symmetry in state space, we immediately arrive at a picture of the state space partitioning, Fig. 13, that is identical to the picture connected with ligand migration, Fig. 1, with the exception of a different naming of the various parts.

Equations (2.7)–(2.10a) then describe the random walk of an ion channel protein in that part of its state space which

corresponds to closed channel states.⁶⁸ It enters that part at R_0 , and stays there until it leaves the shell by crossing the boundary at R_0 again. R_1 corresponds to the size of the full state space, and the relative size of the state space corresponding to the open state is given by $(R_0/R_1)^d$, d being the state space dimension. Using an outer boundary condition (2.10b) instead of the reflective condition (2.10a) would correspond to a situation where the shell corresponding to closed states is again surrounded by the remaining state space corresponding to open states again. This is not a likely situation here, but would be relevant if a larger number of different macroscopic states were involved.

The conditional probability of observing a channel in the closed state at time t , given that it switched to the closed state at $t=0$, is the probability of finding the random walk at all in the closed states shell at time t , under initial condition (2.7). This is identical to our observable $N(t)$, which was the ligand concentration in the shell in the ligand migration interpretation of the model. As noted above, the observable usually reported in measurements of ion channel fluctuations is the distribution of closing times. Since at time t the proteins that have a dwell time $\tau > t$ contribute to $N(t)$, this quantity is connected to the distribution of dwell times $P_{\text{closed}}(\tau)$ via

$$N(t) = \int_t^{\infty} d\tau P_{\text{closed}}(\tau), \quad (6.1)$$

the closed-state time distribution is given by

$$P_{\text{closed}}(t) = -\frac{d}{dt} N(t). \quad (6.2)$$

A number of recent studies^{62,66,69–74} undertake to explain the $t^{-3/2}$ closed-state time distribution observed in many ion channel proteins. In those studies mainly one-dimensional models were considered. Lauger's microscopic defect diffusion model⁶² and Doster *et al.*'s percolation model⁷³ are notable exceptions. However, the latter authors assume that the random walk is restricted to the largest cluster of a bond percolation system, and the nature of the state space partitioning remains very unclear in their work.

In all of these models a discrete configuration space was employed. Although such an approach may give results different from our continuous model if a small number of states are involved, the results will be qualitatively equivalent for a large number of states. Incidentally, the latter case is just the limit for which the $t^{-3/2}$ distribution is obtained in those models.^{66,62}

Few-state-models, on the other hand, employed usually for an analysis of ion channel experiments,^{75,76,77} are motivated mainly by multiexponential fits to data.⁷⁸ It is well-known, that few-state models are able to reproduce quite complicated behavior,⁷⁶ provided the number of parameters is large enough, see also the discussion in Refs. 79, 80, 81. However, such models do not provide any insight into ion channel fluctuations, since they are not based on an understanding of microscopic protein dynamics. Our approach, on

the other hand, provides a route for systematically investigating effects of state space dimensionality, which is not possible in few-state models.

In light of our results in Sec. IV, i.e., the $N(t) \propto t^{-1/2}$ behavior for wide parameter regimes, and the connection of $N(t)$ and $P_{\text{closed}}(t)$ via Eq. (6.2), it is no surprise that one-dimensional models reproduce the $t^{-3/2}$ closed-time distribution. Any description that models the patch of closed states in configuration space as a one-dimensional interval will exhibit this behavior.

However, our results for general dimensions raises the caveat that one should not take this finding as a proof for the one-dimensional structure of the effective ion channel state space. Models employing higher-dimensional state spaces also arrive at the same closed-time distribution for a wide range of parameter values. The particular properties of the actual protein configuration space will be reflected only in *deviations* from the algebraic behavior, the plateau regime being one important signature for that. We note, in closing, that the “tether-ball” model,⁸² advocated recently—on the basis of site-directed mutagenesis experiments—for the inactivation of certain ion channels,^{83,84} belongs to the class of models that exhibit a state space with a dimension $d > 1$.

VII. SUMMARY AND DISCUSSION

We have shown that the appearance of a $t^{-1/2}$ regime for the unreacted fraction $N(t)$ in a reaction–diffusion process described in Eqs. (2.7)–(2.10) is quite robust and independent of the space dimensionality of the process. It will appear whenever there exists a diffusion region of shell-like structure of sufficient width, controlled by an inner reactive boundary condition. Due to the independence of space dimension, one can conclude that the detailed form of the outer boundary is irrelevant for the appearance of the algebraic regime. The insensitivity of these results to space dimension provides also *a posteriori* support for our modeling the ligand diffusion process as isotropic. Clearly, the protein matrix itself is far from isotropic, but it is important to note that there exist universal results for the time-dependence of the decay of $N(t)$ which are *independent* of even relatively gross features of the model.

We saw in Sec. III that for an absorbing inner boundary and no outer boundary, $N(t)$ shows a $t^{-1/2}$ decay in one dimension. In two dimensions the decay of $N(t)$ is logarithmic, while in higher dimensions $N(\infty)$ assumes a nonzero value, the Polya limit. Nevertheless, the final decay to that limit is algebraic, with an exponent $(d-2)/2$. Incidentally, that exponent is again $1/2$ in three dimensions. However, in the geometry discussed in the preceding paragraph, absorption in the boundary layer—effectively a $1d$ situation—dominates the algebraic part of the overall decay of $N(t)$. Numerical support of this claim was given in Sec. IV B, for dimensions one through eight inclusive. An analytical proof, along with an analysis of the conditions under which the result breaks down, was given in Sec. IV C.

Therefore, the existence of an algebraic $t^{-1/2}$ regime in the decay of the ligand fraction $N(t)$ in ligand migration and

rebinding experiments is by no means conclusive evidence for a $1d$ process taking place. On the contrary, such an algebraic decay gives no information on the space dimensionality of the process, as we have shown.

However, there is a clear experimental signature which differentiates between one-dimensional diffusion and an effectively higher-dimensional process; we have demonstrated that the observation of a plateau in a log–log plot of $N(t)$ vs t following the algebraic decay regime indicates that the diffusion path of the ligand is effectively higher-dimensional. Its existence is controlled mainly by the effective dimensionality of the diffusion shell, i.e., the parameters d and X , see Sec. IV D. We note that plateau-like regimes in $N(t)$ have already been observed, but have been attributed partly to escape into the solvent (processes III and IV of Austin *et al.*,¹ see also Refs. 85, 86). Our results indicate that these regimes could also be a signature of the three-dimensionality of the ligand migration process.

The existence of the plateau in dimensions three and higher can be directly related to Polya’s result of nonreturn of an unbiased random walker to the origin in dimensions three and higher. An analysis of this claim was presented in Secs. IV C, IV D, and V. In two dimensions the plateau, or in this case “pseudo-plateau,” is attributable to the marginal logarithmic decay of probability in two dimensions.

Our model and results can also be used to analyze the closing time distribution in ion channel fluctuations, as described briefly in Sec. VI. A full treatment of this topic will be the subject of a separate paper.

ACKNOWLEDGMENTS

The work of D.L.S. was supported in part by the DOE under Grant No. DE-FG03-93ER25155 at the University of Arizona. Much of the work in this paper was done during collaborative visits, funded by a NATO Collaborative Research Grant, which the authors gratefully acknowledge.

¹R. H. Austin, K. W. Beeson, L. Eisenstein, H. Frauenfelder, and I. C. Gunsalus, *Biochemistry* **14**, 5355 (1975).

²N. Alberding, S. S. Chan, L. Eisenstein, H. Frauenfelder, D. Good, I. C. Gunsalus, T. J. Nordlund, M. F. Perutz, A. H. Reynolds, and L. B. Sorensen, *Biochemistry* **17**, 43 (1978).

³D. Beece, L. Eisenstein, H. Frauenfelder, D. Good, M. C. Marden, L. Reinisch, A. H. Reynolds, L. B. Sorensen, and K. T. Yue, *Biochemistry* **19**, 5147 (1980).

⁴A. Ansari, J. Berendzen, S. F. Bowne, H. Frauenfelder, I. E. T. Iben, T. B. Sauke, E. Shyamsunder, and R. D. Young, *Proc. Natl. Acad. Sci. USA* **82**, 5000 (1985).

⁵A. Ansari, E. DiIorio, D. Dlott, H. Frauenfelder, I. E. T. Iben, P. Langer, H. Roder, T. B. Sauke, and E. Shyamsunder, *Biochemistry* **25**, 3139 (1986).

⁶A. Ansari, J. Berendzen, D. Braunstein, B. R. Cowen, H. Frauenfelder, M. K. Hong, I. E. T. Iben, J. B. Johnson, P. Ormos, T. B. Sauke, R. Scholl, A. Schulte, P. J. Steinbach, J. Vittitow, and R. D. Young, *Biochemistry* **26**, 337 (1987).

⁷H. Frauenfelder, N. A. Alberding, A. Ansari, D. Braunstein, B. R. Cowen, M. K. Hong, E. Icko, B. J. Johnson, S. Luck, M. C. Marden, J. R. Mourant, P. Ormos, L. Reinisch, R. Scholl, A. Schulte, E. Shyamsunder, L. B. Sorensen, P. J. Steinbach, A. Xie, R. D. Young, and K. T. Yue, *J. Phys. Chem.* **94**, 1024 (1990).

⁸D. A. Case and M. Karplus, *J. Mol. Biol.* **132**, 343 (1979).

⁹N. Agmon and J. J. Hopfield, *J. Chem. Phys.* **78**, 6947 (1983).

¹⁰N. Agmon and J. J. Hopfield, *J. Chem. Phys.* **79**, 2042 (1983).

- ¹¹H. Frauenfelder, *Naturwissens. Rund.* **38**, 311 (1985).
- ¹²W. Doster, Ch. Holtzhey, H. Miesmer, F. Post, and R. A. Tahir-Kheli, *J. Biol. Phys.* **17**, 281 (1990).
- ¹³W. Nadler and D. L. Stein, *Proc. Natl. Acad. Sci. USA* **88**, 6750 (1991).
- ¹⁴Related work on the $t^{-1/2}$ law in 3d was done independently in J. B. Miers, J. C. Postlewaite, T. Zyung, S. Chen, G. R. Roomig, X. Won, D. D. Dlott, and A. Szabo, *J. Chem. Phys.* **93**, 8771 (1990); however, these authors discuss binding to protoheme in solution, i.e., heme without the protein shell, rather than the ligand migration process.
- ¹⁵C. D. Levermore, W. Nadler, and D. L. Stein, *Phys. Rev. E* **51**, 2779 (1995).
- ¹⁶S. D. Druger, M. A. Ratner, and A. Nitzan, *Phys. Rev. B* **31**, 3939 (1985).
- ¹⁷M. Sahimi, B. D. Hughes, L. E. Scriven, and H. T. Davis, *J. Chem. Phys.* **78**, 6849 (1983).
- ¹⁸A. K. Harrison and R. Zwanzig, *Phys. Rev. A* **32**, 1072 (1985).
- ¹⁹R. Hilfer and R. Orbach, *Chem. Phys.* **128**, 275 (1988).
- ²⁰A. Perera, B. Gaveau, M. Moreau, and K. A. Penson, *Phys. Lett. A* **159**, 158 (1991).
- ²¹R. Zwanzig, *Chem. Phys. Lett.* **164**, 639 (1989).
- ²²M. Tachiya, *J. Chem. Phys.* **70**, 238 (1979); *Rad. Phys. Chem.* **21**, 167 (1983).
- ²³A. Szabo, D. Soup, S. H. Northrup, and J. A. McCammon, *J. Chem. Phys.* **77**, 4484 (1982).
- ²⁴B. I. Hunt and J. G. Powles, *Proc. Phys. Soc.* **88**, 513 (1966).
- ²⁵W. Feller, *Probability and its Applications* (Wiley, New York, 1971), Vol. 2.
- ²⁶A. Szabo, K. Schulten, and Z. Schulten, *J. Chem. Phys.* **72**, 4350 (1980).
- ²⁷K. Schulten, Z. Schulten, and A. Szabo, *J. Chem. Phys.* **74**, 4426 (1981).
- ²⁸W. Nadler and K. Schulten, *J. Chem. Phys.* **82**, 151 (1985).
- ²⁹H. S. Carslaw and J. C. Jaeger, *Conduction of Heat in Solids* (Oxford University, Oxford, 1959).
- ³⁰J. Crank, *The Mathematics of Diffusion* (Oxford University, Oxford, 1975).
- ³¹N. Agmon, *J. Chem. Phys.* **81**, 2811 (1984).
- ³²M. J. Lighthill, *Introduction to Fourier Analysis and Generalized Functions* (Cambridge University, Cambridge, 1958).
- ³³M. Abramowitz and I. A. Stegun, *Handbook of Mathematical Functions* (Dover, New York, 1972).
- ³⁴H. Sano and M. Tachiya, *J. Chem. Phys.* **71**, 1276 (1979).
- ³⁵See, for example, G. Arfken, *Mathematical Methods for Physicists* (Academic, New York, 1966).
- ³⁶I. S. Gradshteyn and I. M. Ryzhik, *Tables of Integrals, Series, and Products*, corrected and enlarged edition (Academic, New York, 1980).
- ³⁷W. H. Press, S. A. Teukolsky, W. T. Vetterling, and B. P. Flannery, *Numerical Recipes* (Cambridge University, Cambridge, 1992).
- ³⁸W. Nadler and K. Schulten, *J. Chem. Phys.* **84**, 4015 (1986).
- ³⁹E. Pines, D. Huppert, and N. Agmon, *J. Chem. Phys.* **88**, 5620 (1988).
- ⁴⁰M. Tachiya (private communication).
- ⁴¹A. Brünger, R. Peters, and K. Schulten, *J. Chem. Phys.* **82**, 2147 (1985).
- ⁴²H.-U. Bauer, K. Schulten, and W. Nadler, *Phys. Rev. B* **38**, 445 (1988).
- ⁴³This follows from Koenig's theorem, a very general result on the zeros of Padé approximants; see A. S. Housholder, *The Numerical Treatment of a Single Nonlinear Equation* (McGraw-Hill, New York, 1970).
- ⁴⁴C. W. Gardiner, *Handbook of Stochastic Methods* (Springer, Berlin, 1983).
- ⁴⁵H. Risken, *The Fokker-Planck Equation* (Springer, Berlin, 1984).
- ⁴⁶N. G. van Kampen, *Stochastic Processes in Physics and Chemistry* (North-Holland, Amsterdam, 1992).
- ⁴⁷H. Frauenfelder, G. A. Petsko, and D. Tsernoglou, *Nature* **280**, 558 (1979).
- ⁴⁸H. Frauenfelder, in *Structure and Dynamics: Nucleic Acids and Proteins*, edited by E. Clementi and R. H. Sarma (Adenine, New York, 1983), p. 369–376.
- ⁴⁹H. Frauenfelder, in *Structure and Motion: Membranes, Nucleic Acids and Proteins*, edited by E. Clementi and R. H. Sarma (Adenine, New York, 1985), p. 205–217.
- ⁵⁰B. Hille, *Ionic Channels and Excitable Membranes* (Sinauer, Sunderland MA, 1984).
- ⁵¹B. Hille, in *The Harvey Lectures, Series 82*, (Alan R. Liss Inc. 1988), p. 47–69.
- ⁵²D. L. Stein, *Spin Glasses and Biology* (World Scientific, Singapore, 1992).
- ⁵³C. M. Newman and D. L. Stein, *Ann. Inst. Henri Poincaré* **31**, 249 (1995).
- ⁵⁴D. Stauffer and A. Aharony, *Introduction to Percolation Theory*, 2nd ed. (Taylor and Francis, London, 1992).
- ⁵⁵H. Frauenfelder, S. G. Sligar, and P. Wolynes, *Science* **254**, 1598 (1991).
- ⁵⁶S. A. Kauffman, *Origins of Order* (Oxford University, Oxford, 1993).
- ⁵⁷R. G. Palmer, *Adv. Phys.* **31**, 669 (1982); *Heidelberg Colloquium on Spin Glasses*, edited by J. L. van Hemmen and I. Morgenstern (Springer, Berlin, 1983), pp. 234–251.
- ⁵⁸D. L. Stein and C. M. Newman, *Phys. Rev. E* **51**, 5228 (1995).
- ⁵⁹P. A. Ferrari, S. Goldstein, and J. L. Lebowitz, in *Statistical Physics and Dynamical Systems, Rigorous Results*, edited by J. Fritz, A. Jaffe, and D. Szász (Birkhäuser, Boston, 1985), pp. 405–441.
- ⁶⁰R. Zwanzig, *Proc. Natl. Acad. Sci. USA* **85**, 2029 (1988).
- ⁶¹W. Nadler and K. Schulten, *Proc. Natl. Acad. Sci. USA* **81**, 5719 (1984).
- ⁶²P. Läger, *Biophys. J.* **53**, 877 (1988).
- ⁶³*Single-Channel Recording*, edited by B. Sakman and E. Neher (Plenum, New York, 1983).
- ⁶⁴L. S. Liebovitch and J. M. Sullivan, *Biophys. J.* **25**, 979 (1987).
- ⁶⁵R. McGee Jr., M. S. P. Sansom, and P. N. R. Usherwood, *J. Memb. Biol.* **102**, 21 (1988).
- ⁶⁶G. L. Millhauser, E. E. Salpeter, and R. E. Oswald, *Proc. Natl. Acad. Sci. USA* **85**, 1503 (1988).
- ⁶⁷G. L. Millhauser, E. E. Salpeter, and R. E. Oswald, *Biophys. J.* **54**, 1165 (1988).
- ⁶⁸We note that the justification of the use of boundary conditions (2.9) and (2.10b) for the description of random walks that cross from one partition to another is by no means trivial. A naive derivation of a such a boundary condition, e.g., starting from a discretized description and going to the continuum limit, would result in a fully absorptive boundary condition at R_0 ; compare Eq. (2.10a). However, together with the initial condition (2.7) that does not make much sense: $N(t)$ would be zero for all times. Nevertheless, in principle, such a boundary condition is correct: almost all random walks will enter the partition only for an infinitesimally short time, and then leave it again across the boundary they came. The walks we are concerned with, on the other hand, are only those which can be recognized to have entered the state space partition, i.e., they must have entered for some time long enough so that the proteins can be recognized experimentally as closed channels. Since it is only this subclass of random walks that we want to describe, we end up with the reactive boundary condition (2.5), or Eq. (2.9) after rescaling. This discussion also makes clear that the parameter γ , and, therefore, the time and length scales τ_r and l_r are connected to the experimental time resolution.
- ⁶⁹G. L. Millhauser, *Biophys. J.* **57**, 857 (1990).
- ⁷⁰R. E. Oswald, G. L. Millhauser, and A. Carter, *Biophys. J.* **57**, 857 (1991).
- ⁷¹C. A. Condat, *Phys. Rev. A* **39**, 2112 (1989).
- ⁷²C. A. Condat and J. Jäckle, *Biophys. J.* **55**, 915 (1989).
- ⁷³W. Doster, W. Schirmacher, and M. Settles, *Biophys. J.* **57**, 681 (1990).
- ⁷⁴L. S. Liebovitch, L. Y. Selector, and R. P. Kline, *Biophys. J.* **63**, 1579 (1992).
- ⁷⁵S. J. Korn, and R. Horn, *Biophys. J.* **54**, 871 (1988).
- ⁷⁶O. B. McManus, D. S. Weiss, C. E. Spivak, A. L. Blatz, and K. L. Magleby, *Biophys. J.* **54**, 859 (1988).
- ⁷⁷J. D. Becker, J. Honerkamp, J. Hirsch, U. Fröbe, and R. Greger, *Eur. J. Physiol. (Pflügers Arch.)* **426**, 328 (1994).
- ⁷⁸D. Colquhoun and F. J. Sigworth, in Ref. 63, p. 191–263.
- ⁷⁹L. S. Liebovitch, *Biophys. J.* **55**, 373 (1989).
- ⁸⁰R. Horn and S. J. Korn, *Biophys. J.* **55**, 379 (1989).
- ⁸¹O. B. McManus, C. E. Spivak, A. L. Blatz, D. S. Weiss, and K. L. Magleby, *Biophys. J.* **54**, 383 (1989).
- ⁸²C. M. Armstrong and F. Bezanilla, *J. Gen. Physiol.* **70**, 567 (1977).
- ⁸³T. Hoshi, W. N. Zagotta, and R. W. Aldrich, *Science* **250**, 533 (1990).
- ⁸⁴W. N. Zagotta, T. Hoshi, and R. W. Aldrich, *Science* **250**, 568 (1990).
- ⁸⁵M. K. Hong, E. Shyamsunder, and R. H. Austin, *Phys. Rev. Lett.* **66**, 2673 (1991).
- ⁸⁶W. D. Tian, J. T. Sage, V. Srajer, and P. M. Champion, *Phys. Rev. Lett.* **68**, 408 (1992).